ANNUAL REVIEWS

Annual Review of Earth and Planetary Sciences

Petrogenesis and Geodynamic Significance of Xenolithic Eclogites

Sonja Aulbach[1] and Katie A. Smart[2]

[1]Institut für Geowissenschaften, Goethe Universität, Frankfurt am Main, Germany; email: s.aulbach@em.uni-frankfurt.de

[2]Department of Geosciences, University of Tromsø, The Arctic University of Norway, Tromsø, Norway; email: kathleen.a.smart@uit.no

Annu. Rev. Earth Planet. Sci. 2023. 51:521–49

First published as a Review in Advance on February 15, 2023

The *Annual Review of Earth and Planetary Sciences* is online at earth.annualreviews.org

https://doi.org/10.1146/annurev-earth-031621-112904

Keywords

kimberlite-borne xenolithic eclogites, paleo-subduction zones, lithospheric mantle, convecting mantle, continent evolution, deep geochemical cycles

Abstract

Kimberlite-borne xenolithic eclogites, typically occurring in or near cratons, have long been recognized as remnants of Precambrian subducted oceanic crust that have undergone partial melting to yield granitoids similar to the Archean continental crust. While some eclogitized oceanic crust was emplaced into cratonic lithospheres, the majority was deeply subducted to form lithologic and geochemical heterogeneities in the convecting mantle. If we accept that most xenolithic eclogites originally formed at Earth's surface, then their geodynamic significance encompasses four tectonic environments: (*a*) spreading ridges, where precursors formed by partial melting of convecting mantle and subsequent melt differentiation; (*b*) subduction zones, where oceanic crust was metamorphosed and interacted with other slab lithologies; (*c*) the cratonic mantle lithosphere, where the eclogite source was variably modified subsequent to emplacement in Mesoarchean to Paleoproterozoic time; and (*d*) the convecting mantle, into which the vast majority of subduction-modified oceanic crust not captured in the cratonic lithosphere was recycled.

- Xenolithic eclogites are fragments of ca. 3.0–1.8 Ga oceanic crust and signal robust subduction tectonics from the Mesoarchean.
- Multiple constraints indicate an origin as variably differentiated oceanic crust, followed by subduction metamorphism, and prolonged mantle residence.

- Xenolithic eclogites thus permit investigation of deep geochemical cycles related to recycling of Precambrian oceanic crust.
- They help constrain asthenosphere thermal plus redox evolution and contribute to cratonic physical properties and mineral endowments.

Xenolith: the physical sample available for study that has been plucked by the host kimberlite from the cratonic mantle wall rock—the mantle eclogite source

Cratonic/continental lithospheric mantle: thick (up to ~250 km) region of relatively cool, chemically depleted, and rigid nonconvecting mantle that underlies coherent blocks of Precambrian continental shields and usually includes Archean-aged crust ± lithospheric mantle cores surrounded by Proterozoic blocks

Xenocrysts: single mineral grains, notably including diamond, derived from the disaggregation of xenoliths during turbulent transport in the host magma, to which they are genetically unrelated

Protolith: the precursor, original rock before any metamorphic or metasomatic reactions occurred to form the final rock; for xenolithic eclogite, the protoliths are mafic volcanic rocks, such as basalts or picrites, and their intrusive counterparts, such as gabbros

1. INTRODUCTION

Eclogite is a metamorphic rock of broadly basaltic composition defined by the absence of plagioclase and presence of >75 vol% omphacite and garnet (neither of which is >70%) and is eponymous with the high- to ultra-high-pressure medium-temperature metamorphic facies (Tsujimori & Mattinson 2021). The observation of high-grade metamorphic rocks, such as eclogites, at Earth's surface requires exhumation from great depths, involving two principal mechanisms: as part of tectonically exhumed terranes (orogenic eclogites) or as accidental fragments (xenoliths) entrained in mantle-derived magmas (Tsujimori & Mattinson 2021). Tectonic exhumation occurs in collisional or accretionary settings and is a slow process that may be accompanied by retrograde reactions where, for dynamic reasons, material from only <80–100 km depth is typically returned to the surface in convergent margins (Bebout 2014). Conversely, with rare exceptions, xenolithic eclogites are exhumed in fast-ascending, small-volume, incompatible element–rich carbonated melts (principally kimberlites and lamproites; to simplify, only kimberlite is referred to hereafter), which intrude old continental interiors (cratons) and their margins (Jacob 2004).

Kimberlites are emplaced into Earth's crust in a matter of hours or days; during their ascent through cold and refractory cratonic/continental lithospheric mantle, kimberlites can exhume wall rock material from 250 km depth and more (e.g., Brett et al. 2015). Kimberlite magmas are considered primary diamond sources (Gurney et al. 2010), and studies of mantle xenoliths, diamonds, and their inclusions are closely intertwined. Monocrystalline diamonds are xenocrysts (i.e., not genetically related) in kimberlite magmas (Richardson et al. 1984) and occasionally found in situ in mantle xenoliths, including eclogite (e.g., Deines et al. 1991, Ireland et al. 1994, Viljoen 1995). These diamonds carry inclusions with mineralogies and compositions similar to those of their mantle source rocks (Meyer 1987). Due to the antiquity and chemical inertness of their diamond host, inclusions represent the early and deep record of the origin and evolution of eclogitic mantle sources and are therefore a complementary source of information to xenolithic eclogites (Stachel et al. 2022). Kimberlite-borne xenolithic eclogites—often also referred to in the literature as mantle eclogites—are the focus of this review; their diamond-hosted counterparts are used for comparison to highlight aspects of eclogite origin and evolution.

A plethora of mineralogical, geochemical, and isotopic evidence indicates that most kimberlite-borne xenolithic eclogite suites, for which Paleoproterozoic to Archean ages are commonly determined, had protoliths that originated at low pressures and temperatures (e.g., Helmstaedt & Schulze 1989, Jacob 2004). Consequently, xenolithic eclogites are widely interpreted to have originally formed within the oceanic crust (discussed in more detail in Section 3.3) and to have been recycled to mantle depths during the closure of paleo-ocean basins that accompanies protocontinent amalgamation during craton formation (e.g., Shirey & Richardson 2011). Indeed, xenolithic eclogites have been linked to the formation of tonalite-trondhjemite-granodiorite (TTG) rocks that comprise large parts of cratons because they yield granitoid melts during subduction under generally hotter Archean mantle conditions (e.g., Ireland et al. 1994). The paleo-oceanic crust rock record, as preserved by orogenic eclogites and the oceanic crustal portions of ophiolites, becomes sparser and its origins more controversial in deep time (e.g., Waterton et al. 2022), such

that xenolithic eclogites may well represent our main, if not only, samples of ancient oceanic crust (Foley 2011). Thus, xenolithic eclogites and their constituents are singularly useful archives of ancient geodynamics: from formation at paleo-spreading ridges through seawater alteration, subduction, and metamorphism to their selective emplacement in growing cratons and ultimately deep subduction into convecting mantle sources that have been sporadically tapped by deeply derived magmas [komatiites, ocean island basalts (OIBs)] through time.

The use of the xenolithic eclogite record to obtain constraints on the physicochemical conditions in the above geodynamic environments hinges on accurately deciphering the petrogenesis of each individual sample, which reflects variable superposition of multiple processes occurring between emplacement of oceanic crust into the lithosphere and entrainment in kimberlites, often billions of years later. The aims of this review are to (*a*) assess the approaches and challenges inherent in determining physicochemical properties and ages of xenolithic eclogite; (*b*) synthesize the current understanding of eclogite petrogenesis; (*c*) highlight the utility of eclogite for addressing various aspects of terrestrial dynamics, ranging from long-standing and widely accepted insights to emerging and more controversial applications; and (*d*) identify knowledge gaps and potential future uses of this uniquely beautiful and valuable rock, which may further inform models of early and deep Earth processes, the effects of which trickle through to the present day.

Oxygen fugacity (fO_2): intensive parameter related to the chemical potential of oxygen, μO_2, typically reported in log 10 units relative to a buffering assemblage, such as fayalite-magnetite-quartz

2. CLASSIFICATION, PHYSICOCHEMICAL PROPERTIES, AND AGES OF XENOLITHIC ECLOGITES

In order to ascertain the petrogenesis of xenolithic eclogites, they must be identified and classified, their mineral compositions determined, and, critically, their bulk compositions reconstructed. The procedures behind eclogite classification, which broadly reflects their origin as various parts of oceanic crust, and calculation of bulk-rock compositions are detailed in the **Supplemental Text**, which also includes information on more unusual eclogite xenolith occurrences with respect to host rock and/or dynamic setting that are not included in this review. Broadly, eclogites are divided into those with gabbroic protoliths [whole-rock $Eu/Eu^* > 1.05$ (see **Supplemental Text**)] interpreted as plagioclase-rich cumulates and those with basaltic protoliths ($Eu/Eu^* \leq 1.05$) interpreted as residual melts (**Figure 1*a***) that may also be picritic in composition. Basaltic eclogites are divided into high-Ca and high-Mg eclogites, with major element characteristics suggestive of representing more and less differentiated extrusives (**Figure 1*b***). However, high-Mg eclogites may have a multitude of origins reflecting partial melt loss, metasomatism by kimberlite-like melt, or eclogite-peridotite interactions, all of which increase MgO contents (**Supplemental Text**). High-Fe eclogites have an uncertain origin, possibly linked to an Fe-rich protolith. Bulk-rock reconstruction is important to avoid the ubiquitous presence of kimberlite material in the grain boundary component that will be analyzed during routine bulk-rock analyses (e.g., Barth et al. 2001) and mask protolith compositions. In this context, it is important to consider that it is difficult to constrain the petrogenesis of xenolithic eclogites from one mineral alone—for example, when only xenocryst material is available—due to strong temperature and crystal-chemical effects on the minor and trace element distribution between the constituent minerals (**Figure 1*c***).

Supplemental Material >

In order to use xenolithic eclogites as paleo-geodynamic archives, we must assess their physical state [pressure (P), temperature (T), and oxygen fugacity (fO_2)] at the time of entrainment and constrain their ages. This is no trivial undertaking because xenolithic eclogite is a high-variance system, often consisting of garnet and omphacite-rich clinopyroxene only, and typically inclusion-poor to inclusion-free. The **Supplemental Text** reviews the geothermobarometers and oxybarometers as well as dating tools available to researchers and the challenges and uncertainties associated with their use. Xenolithic eclogites and related xenocrysts occur on most cratons and, therefore, the information drawn from xenolithic eclogites has global rather than regional

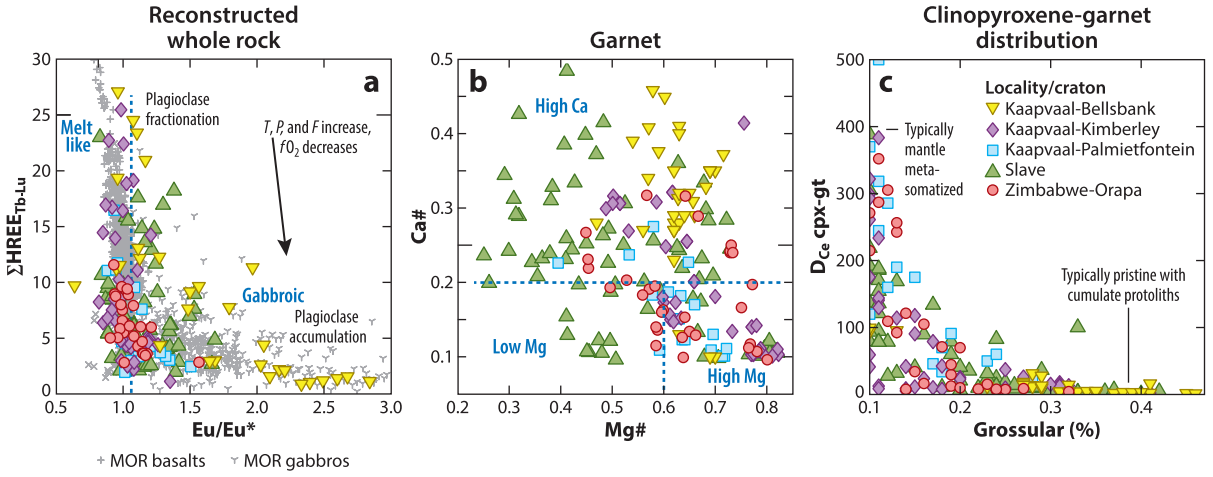

Figure 1

Classification of eclogite and pyroxenite xenoliths from selected localities (see the **Supplemental Text** and data sources in **Supplemental Table 1**). (*a*) Heavy rare earth element (HREE) abundances (ΣHREE; ppm, summed from Tb to Lu) as a function of Eu/Eu* [chondrite-normalized Eu/(Sm*Gd)$^{0.5}$ > 1.05 (Rudnick & Fountain 1995) (chondrite values from McDonough & Sun 1995)] distinguishing gabbroic from nongabbroic or melt-like protoliths, which have plagioclase-rich and residual protoliths, respectively. (*b*) Mg# [Mg/(Mg + Fe^{total}) molar] versus Ca# [Ca/(Ca + Mg + Fe^{total} + Mn) molar] in garnet further distinguishing high-Mg, low-Mg, and high-Ca eclogites according to Aulbach & Jacob (2016). Higher mantle potential temperatures and lower oxygen fugacity (fO_2) in the Archean when the protoliths to many eclogite xenoliths formed, imply higher melt fractions (F) and lower concentrations of incompatible elements, such as REEs, and possibly slightly higher Eu/Eu* in the parental melt (Aulbach & Jacob 2016) than in modern mid-ocean ridge basalts (MORBs), as shown qualitatively by the arrow in panel *a*. Shown for comparison are modern MORB (Jenner & O'Neill 2012) and mid-ocean ridge (MOR) gabbros [Eu/Eu* > 1.05 (from PetDB; Lehnert et al. 2000)]. (*c*) Distribution (D) of Ce between clinopyroxene (cpx) and garnet (gt) as a function of grossular content (i.e., cpx Ce/gt Ce), illustrating the strong dependence of incompatible element uptake in garnet on CaO content.

Supplemental Material >

implications (**Figure 2**). Moreover, they were entrained from a large pressure interval of the lithospheric mantle (**Figure 3*a***) and display a wide range of fO_2 that entails variable speciation of several multivalent elements, such as Fe, V, Eu, and Cr (**Figure 3*c***). Finally, eclogites have predominantly Mesoarchean to Paleoproterozoic ages (**Figure 4**) and therefore can be used to illuminate ancient geodynamic processes. The following discussion revisits and thoroughly investigates these topics. In order to clearly present the eclogite data discussed here, the figures in this contribution display a selected eclogite database listed in **Supplemental Table 1**, which comprises well-characterized eclogite suites from the Kaapvaal-Zimbabwe and Slave cratons; other data sources are indicated in the relevant figure captions.

3. PETROGENESIS OF XENOLITHIC ECLOGITE

3.1. Evidence for Crustal Precursors to Xenolithic Eclogite

A brief historical perspective of the debate on the origin of xenolithic eclogites as crystallized high-pressure melts versus subducted oceanic crust is provided in the **Supplemental Text**. Several review papers have over the years collated arguments in favor of the latter origin of xenolithic eclogite (e.g., Jacob 2004, Aulbach & Jacob 2016), including but not limited to (*a*) the occurrence of minerals not stable on the liquidus of mafic melts in the mantle, such as quartz/coesite and kyanite; (*b*) the presence of strong positive/negative Eu anomalies that are unlikely to be generated by redox effects in the mantle and require the accumulation/fractionation of plagioclase at much lower pressures than those from which xenolithic eclogites are entrained (**Figure 1*a***);

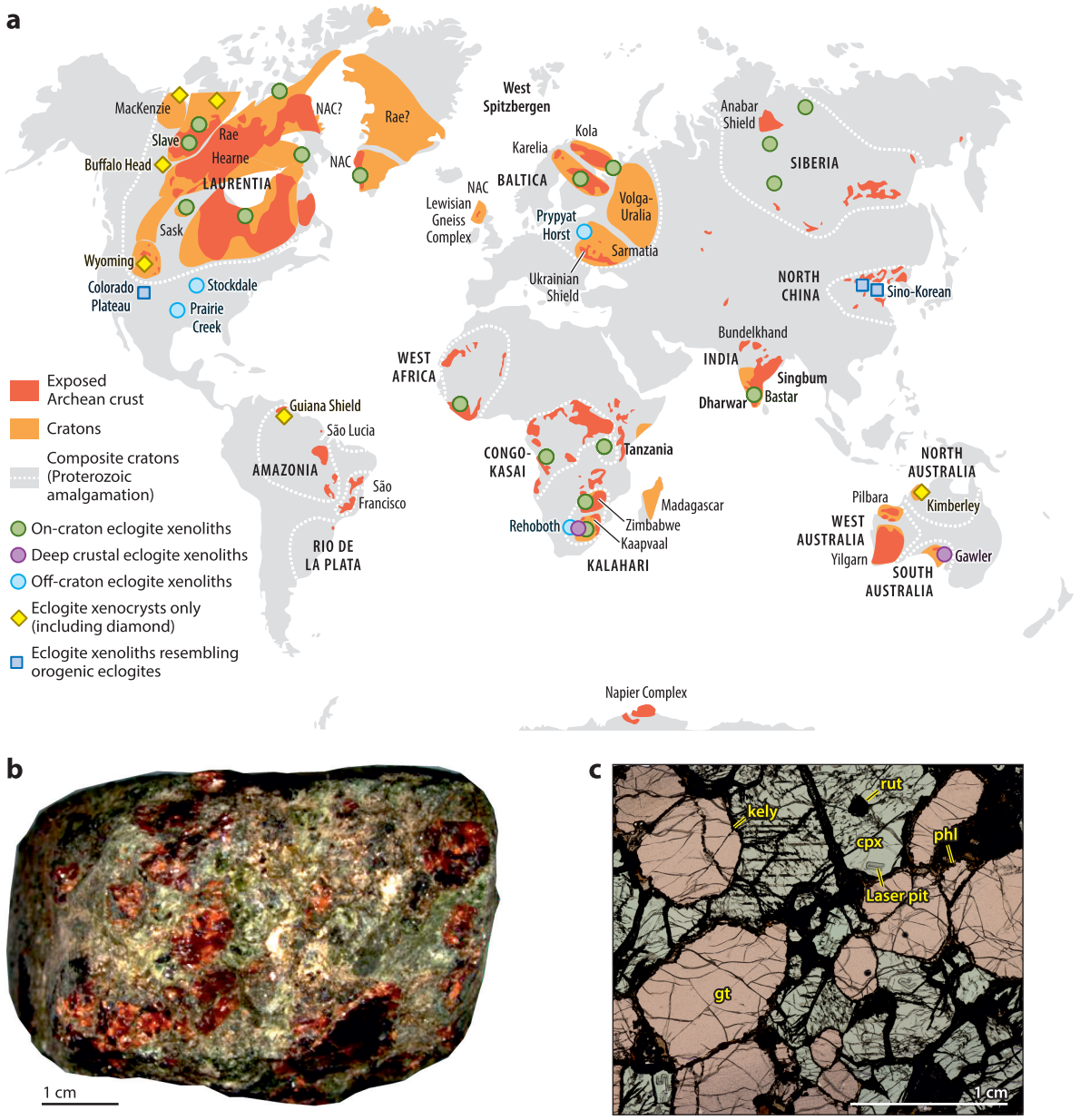

Figure 2

Geographic distribution and petrography of eclogite and pyroxenite xenoliths and their disaggregation products. (*a*) Map of the world with cratonic and off-cratonic localities where eclogite xenoliths and xenocrysts have been transported to the surface (each dot may represent multiple kimberlite intrusions or fields), mostly by kimberlites and related rocks, rarely by other host rocks (adakite, carbonatite, serpentinized ultramafic breccia) (localities with references are in **Supplemental Table 1** and the **Supplemental Text**). Panel adapted with permission from Pearson & Wittig (2014). (*b*) Photograph and (*c*) thick-section scan (plane-polarized light) of an eclogite xenolith from Koidu in the West African craton, illustrating its appearance at the hand specimen scale, with typical straight-interlocking to curvilinear grain boundaries at the section scale, subequal proportions of garnet (gt) and clinopyroxene (cpx), and accessory rutile (rut). Rim of gt [kelphite (kely); i.e., assemblage of pyroxenes and spinel resulting from breakdown of gt] and cpx are partially altered; the laser ablation pit from Sr isotopic analysis is visible in one cpx grain; secondary phlogopite (phl) is crystallized at grain boundaries and in grain fractures, which are filled with cryptocrystalline kimberlite material. Abbreviation: NAC, North Atlantic Craton.

Supplemental Material >

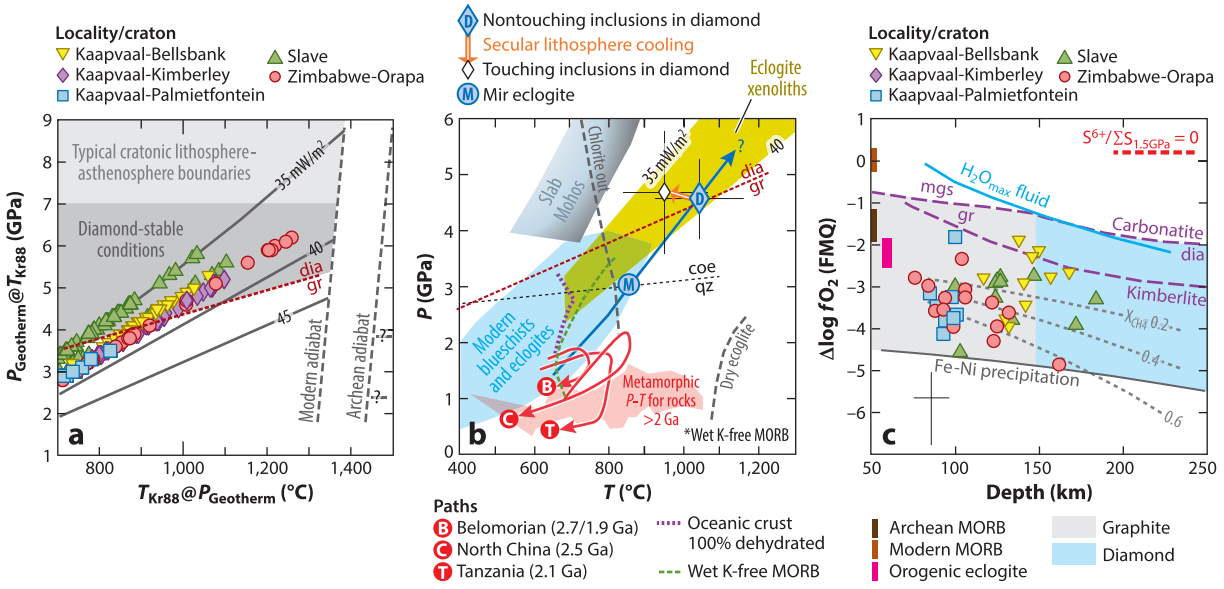

Figure 3

Pressure (*P*) and temperature (*T*) in eclogite and pyroxenite xenoliths (data sources in **Supplemental Table 1**). (*a*) *P* (GPa) versus *T* (°C) obtained as described in the **Supplemental Text**. Also shown are the diamond-graphite (dia-gr) boundary from Day (2012), illustrating that many eclogite xenoliths resided at diamond-stable conditions (*grey field*), and some steady-state conductive geotherms and the modern adiabat after Hasterok & Chapman (2011), which would have been located at a higher range of temperatures in the Archean. Typical cratonic lithosphere-asthenosphere boundaries at 7–9 GPa (Artemieva 2006) are indicated. (*b*) *P* (GPa) versus *T* (°C) diagram after Stachel et al. (2022), with two steady-state conductive geotherms as in panel *a* (shown as *yellow field*), to which the majority of eclogite xenoliths are assumed to have equilibrated. A tentative Archean subduction path (*blue arrow*) is adapted from Stachel et al. (2022, and references therein). Touching inclusions record lower average temperatures, indicative of secular lithosphere cooling (*orange and white arrow*). Shown are *P-T* paths for eclogites from the Belomorian Belt in Russia as above (*red-circled B*), from orogenic eclogites in Tanzania (*red-circled T*) (Möller et al. 1995) and eclogite-facies ophiolite from the central orogenic belt in the North China craton (*red-circled C*) (Ning et al. 2022). Also shown are the coesite-quartz (coe-qz) boundary, chlorite-out curve, and slab Mohos (*gray field*), relevant to dehydration of oceanic mantle; solidus (*dotted line*) for dry (*gray*) and for K-free wet mid-ocean ridge basalt (MORB)-like eclogite (*green*); a curve (*purple*) for 100% dehydration of oceanic crust; modern subduction zone rocks (*blue field*); and the peak *P-T* conditions of metamorphic rocks older than 2 Ga (*pink field*) as in Stachel et al. (2022, and references therein). Panel adapted with permission from Stachel et al. (2022). (*c*) Oxygen fugacity (fO_2) in eclogite and pyroxenite xenoliths (data sources in **Supplemental Table 1**) by locality/craton, calculated using the oxybarometer of Stagno et al. (2015) relative to the fayalite-magnetite-quartz (FMQ) buffer [expressed as $\Delta \log fO_2$ (FMQ)] as a function of depth. Only samples with Si cations per formula units in clinopyroxene ≥1.97 (for 6O) are shown to minimize effects of silica undersaturation (Aulbach et al. 2022); fO_2 values are maxima for remaining samples if not quartz saturated (e.g., Smart et al. 2021a, Aulbach et al. 2022). Also shown are, for conditions along a conductive geotherm corresponding to a surface heat flow of 40 mW/m^2, the stability of carbonatite/magnesite (mgs) versus diamond (dia)/graphite (gr) and of carbonated silicate melt with 10 mol% CO_2 (~kimberlite), the Fe-Ni precipitation curve (~metal saturation) from Stagno et al. (2013), the H_2O maximum curve, and the fO_2-dependent fraction (X) of CH_4 in CHO fluids from Luth & Stachel (2014). The error bar reflects the propagated asymmetrical uncertainty of +1.1/−1.6 on $\Delta \log fO_2$ when uncertainties in *P-T* estimates are added to those inherent in the determination of $Fe^{3+}/\Sigma Fe$ in garnet (Aulbach et al. 2022) and ~±10 km along a conductive cratonic geotherm for an uncertainty of 60°C in *T*. Also shown are estimates for orogenic eclogite from Tianshan under prograde metamorphic conditions (Tao et al. 2020) and modern and Archean MORB (Aulbach et al. 2019).

Supplemental Material >

(*c*) non-mantle stable isotope signatures in garnet ± clinopyroxene (classically $\delta^{18}O$, but in recent years also $\delta^{26}Mg$, $\delta^{44/40}Ca$, and $\delta^{66}Zn$) and sulfide ($\delta^{34}S$) that require low-temperature fractionation at or near the surface, e.g., during seawater alteration (e.g., Korolev et al. 2018, Burness et al. 2021, Smart et al. 2021a, Liu et al. 2022) (**Figure 5*a***; **Supplemental Figure 2**); non-mantle volatile isotope compositions ($\delta^{13}C$, $\delta^{15}N$, $\delta^{34}S$) have also been determined for eclogitic

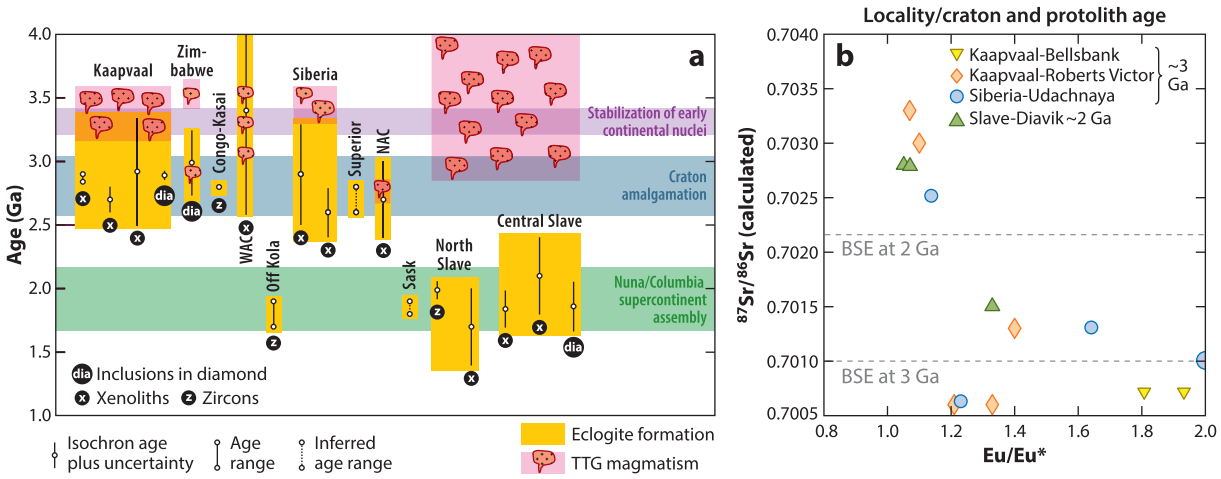

Figure 4

Age constraints for eclogite and pyroxenite xenoliths. (*a*) Summary of age constraints for the formation of cratonic eclogite sources sampled by xenoliths (x) and diamonds (dia), using bulk rocks, mineral separates, or zircons (z) from various cratons or cratonic entities (data sources in **Supplemental Table 1**). Shown for comparison are dominant periods of continental crust formation as recorded in tonalite-trondhjemite-granodiorite rocks forming part of Archean granite-greenstone terranes (Zeh et al. 2009, Tappe et al. 2011, Helmstaedt & Pehrsson 2012, Kostrovitsky et al. 2016, Rollinson 2016, Bolhar et al. 2017). Also shown are the time intervals for the formation of the first nuclei of continental lithosphere (Griffin et al. 2014), Meso- to Neoarchean craton amalgamation leading to consumption of ocean basins and emplacement of oceanic crust during initiation of Wilson cycles (Shirey & Richardson 2011), and amalgamation of the Nuna/Columbia supercontinent (de Oliveira Chaves 2021). Note that most of these ages, in particular if isochron derived, are likely to reflect metamorphism when isotope systems would have been reset, whereas the formation of the oceanic crust would have occurred some tens to hundreds of Ma earlier. (*b*) Calculated initial $^{87}Sr/^{86}Sr$ as a function of Eu/Eu* in eclogite xenoliths (after Aulbach & Arndt 2019a, with additional data from Mikhailenko et al. 2020), whereby those with a strong cumulate character (high Eu/Eu*) tend to retain the least radiogenic Sr. As Rb is difficult to quantify accurately in eclogite minerals, the initial $^{87}Sr/^{86}Sr$ was obtained by estimating $^{87}Rb/^{86}Sr$ from the relationship of Rb/Sr with Eu/Eu* in modern cumulates (see Aulbach & Arndt 2019a). Isotopic composition of BSE at 3 and 2 Ga was calculated forward from initial BSE values (details in Aulbach & Arndt 2019a). When compared to independent age determinations for the various eclogite suites, it is apparent that variably depleted mantle was involved in the formation of their igneous protoliths. Abbreviations: BSE, bulk silicate Earth; NAC, North Atlantic Craton; WAC, West African Craton.

diamond and sulfide contained therein, including mass-independently fractionated S that can only have been generated in the ozone-poor Archean atmosphere (Cartigny et al. 2014, and references therein); (*d*) elemental systematics, such as negatively correlated MgO and Y abundances, or positively correlated TiO_2 and Y abundances that are not permissive of high-pressure fractionation of garnet, which would concentrate MgO and Y but exclude Sm (Aulbach & Arndt 2019a,b) (**Figure 5*b***); and (*e*) evidence for prograde *P-T* paths comparable with thermal gradient trajectories in (warm) modern subduction zones (**Figure 3*b***). Xenolithic eclogites are typically bimineralic and contain unzoned minerals, which generally does not allow *P-T*(-*t*) path determination (where *t* = time). However, both pseudosection modeling of a kyanite-banded eclogite and application of elastic geobarometry to garnet-shielded single perfect quartz crystals resulted in *P-T* paths similar to prograde subduction zone geothermal gradients (Sommer et al. 2017, Alvaro et al. 2020).

Supplemental Material >

None of this excludes, a priori, an origin as foundered mafic continental crust. Oceanic and continental mafic rocks formed in convergent margins have distinct trace element patterns, the latter showing characteristic Ti-Nb-Ta depletions relative to similarly incompatible elements during mantle melting (e.g., Tatsumi et al. 1986). Unfortunately, the accurate determination of these diagnostic elements in xenolithic eclogites is hampered by their concentration in accessory rutile, the modal proportions of which are often not directly determined (**Supplemental Text**).

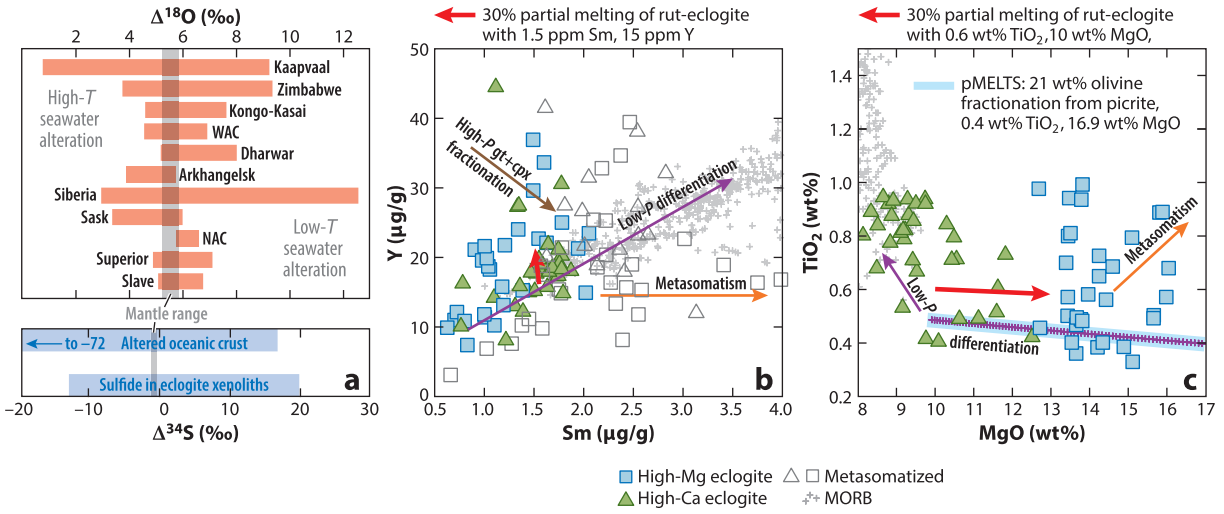

Figure 5

Signatures of a low-pressure (*P*), seawater-altered protolith and of later metasomatism in eclogite xenoliths. (*a*) Stable isotope compositions of minerals in eclogite xenoliths. The top panel summarizes $\delta^{18}O$ (‰) in eclogite xenoliths with ranges after Korolev et al. (2021), plus data for the Sask craton from Czas et al. (2018). The range of mantle $\delta^{18}O$ values is from Mattey et al. (1994), and the effects of low- and high-temperature (*T*) seawater alteration are according to Gregory & Taylor (1981). The bottom panel shows range of $\delta^{34}S$ in sulfides from eclogite xenoliths compared to altered oceanic crust and mantle from Burness et al. (2021). (*b*) Y (µg/g) abundance as a function of Sm (µg/g) abundance in reconstructed bulk eclogite xenoliths; only high-Ca and high-Mg eclogites (from Aulbach & Arndt 2019b), with suggested more and less differentiated melt-like protoliths, respectively, are shown for simplicity. Open symbols indicate metasomatized samples with Ce/Yb > normal mid-ocean ridge basalt (NMORB). The purple arrow shows qualitatively the expected low-*P* differentiation trend, as exhibited by modern mid-ocean ridge basalt (MORB) (*light gray crosses*) (Jenner & O'Neill 2012); the red arrow shows quantitatively the effect of 30% melt extraction (from Aulbach & Arndt 2019b); the brown arrow shows the qualitatively expected trend for fractionation of garnet (gt) and clinopyroxene (cpx) at high *P*; and the orange arrow shows qualitatively the trend of mantle metasomatism. (*c*) TiO_2 content (wt%) in reconstructed bulk eclogite and peridotite xenoliths [including rutile (rut) mass estimated as described in the **Supplemental Text**] as a function of MgO content (wt%). The red arrow is as seen in panel *b*; the differentiation trend for fractionation of only olivine from a picritic staring material (*purple arrow and crosses*) was quantitatively calculated using pMELTS software (Ghiorso et al. 2002; after Aulbach & Arndt 2019b). Panels *b* and *c* adapted with permission from Aulbach & Arndt (2019b). Abbreviations: NAC, North Atlantic Craton; WAC, West African Craton.

Supplemental Material >

Bulk compositions for large xenolithic eclogites reconstructed with measured rutile modes dominantly lack the negative Ti anomaly that might be expected in mafic delaminates, such as lower continental crust or arc basalts (**Figure 6*a***). Moreover, most xenolithic eclogites do not have the high combined MgO and FeO contents (the latter conferring the necessary density enabling delamination) or high SiO_2 and CaO contents (not shown in **Figure 6**) that characterize estimates for the composition of the foundered component (delaminate), such as arc basalts, deep arc cumulates, or mafic lower continental crust (**Figure 6*b***). Even after allowing for light rare earth element (LREE) depletion due to melt extraction, rare earth element (REE) patterns for basaltic xenolithic eclogites do not have the negative slopes in the middle REEs and heavy rare earth elements (HREEs) displayed by most arc cumulates, or by OIBs or mafic lower continental crust that could have foundered and been captured in the mantle lithosphere (**Figure 6*a***; **Supplemental Figure 3**). Finally, triple O isotope systematics in xenolithic eclogite fully overlap those of modern, seawater-altered oceanic crust (McGunnigle et al. 2022), which is difficult to reconcile with a foundered origin. In summary, the weight of the evidence suggests that most gabbroic and basaltic xenolithic eclogites have a common origin via low-pressure differentiation of oceanic crust composed of intrusive and extrusive sections.

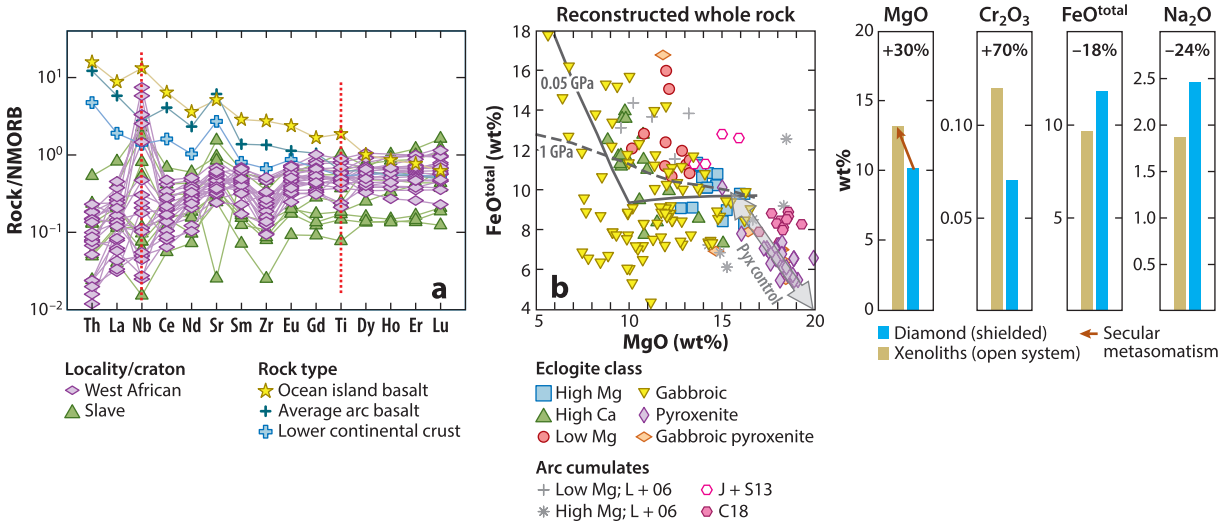

Figure 6

Effects of low-pressure crystallization and mantle metasomatism in bulk eclogite and pyroxenite xenoliths (data sources in **Supplemental Table 1**), and comparison to foundered continental material. (*a*) Normal mid-ocean ridge basalt (NMORB)-normalized trace element patterns for bulk eclogite reconstructions from mineral modes and compositions, including rutile. Rutile modal abundances were determined by point counting [Slave (Aulbach et al. 2007)] or by comparison of measured bulk Ti and garnet-clinopyroxene Ti contents [Koidu, West African craton (Barth et al. 2001)]. Shown for comparison are patterns for bulk lower continental crust (Rudnick & Gao 2014), average arc basalt (Schmidt & Jagoutz 2017), and ocean island basalt (Sun & McDonough 1989); NMORB is from Gale et al. (2013). Both Ti and Nb are highlighted with a dashed line to illustrate that most bulk rocks do not show Ti negative anomalies typifying potential continent-derived foundered or arc material, while Nb is highly variable, reflecting highly variable concentrations in measured rutile combined with a nugget effect related to haphazard exposure of grains in a given section. (*b*) FeO^{total} as a function of MgO (all wt%) by class. Shown for comparison is a suggested pyroxene (pyx) control trend reflecting the addition of a high-temperature pyroxene from a kimberlite-like metasomatic melt (Aulbach et al. 2020). Some high-Mg eclogites and most pyroxenites fall on this trend. Also shown are estimated compositions for a foundered component that would have formed in deep arcs or in deep crustal underplates [L + 06 (from Lee et al. 2006); J + S13 (from Jagoutz & Schmidt 2013); C18 (from Chin 2018)]. Trends for fractional crystallization of a picritic parental melt at 0.05 and 1 GPa are from Aulbach & Jacob (2016) (*thick gray lines*). (*c*) Secular evolution of the mantle eclogite reservoir due to mantle metasomatism, captured by concentrations of various major and minor elements (wt%) in bulk eclogites and pyroxenites reconstructed from inclusions in diamond (shielded) versus xenoliths (open system). The latter was calculated as a composite present-day mantle eclogite/pyroxenite source, using median compositions for each of the six eclogite/pyroxenite classes weighted by their proportion based on nearly 1,000 samples (Stachel et al. 2022); the percentage change is also shown.

3.2. Eclogite Xenolith Petrogenesis in the Context of Earth System Evolution

Although xenolithic eclogites plausibly have mid-ocean ridge basalt (MORB)-like protoliths, secular evolution of the mantle and the ocean-atmosphere system imply that eclogite protoliths differed from the modern oceanic crust. The Archean ambient convecting mantle was warmer (e.g., Herzberg et al. 2010) and possibly more reduced than today (e.g., Foley 2011), which facilitated deeper onset of partial melting and higher melt fraction (F) at ridges, with consequences for the composition and thickness of the oceanic crust (e.g., Herzberg et al. 2010, Asimow 2022). In comparison to modern MORB, Archean oceanic crust was thus picritic, with higher MgO contents (Jacob 2004) and lower incompatible element concentrations due to dilution in higher melt volumes (**Figure 1*a***). Furthermore, the atmosphere was highly reduced until ca. 2.4 Ga, as were the ocean bottom waters until ca. 0.6 Ga (e.g., Lyons et al. 2014), with consequences for the effects of seawater alteration and the speciation, availability, and mobility of polyvalent elements, among

Supplemental Material >

them carbon and sulfur (e.g., Jugo et al. 2005, Evans & Tomkins 2011, Stagno et al. 2013, Stolper & Keller 2018).

Mantle potential temperature (T_P): the temperature a parcel of mantle rock would have at the surface of Earth after adiabatic ascent (where no heat is lost or gained from the mantle parcel), if it lost no partial melt

Finally, subduction geometries and metamorphic reactions in subduction zones depend on thermal gradients (e.g., Schmidt & Poli 2014), which would have been higher in the Precambrian (e.g., Brown & Johnson 2019). A higher Precambrian mantle potential temperature (T_P) would have consequences for the cycling of carbon, water, sulfur, and other elements (Evans & Tomkins 2011, Dasgupta 2013, Magni et al. 2014), as well as the feasibility of slab melting along warmer geotherms allowing the wet eclogite solidus to be crossed (**Figure 3*b***). In addition to changing physicochemical conditions, MgO contents of the oceanic crust also affected the prograde metamorphic reaction sequence and mineralogy of the slab upon subduction, resulting in Archean subduction zones that were characterized by different facies progressions and mineral assemblages than observed in classic low-*T*/high-*P* subduction terranes (Palin & Dyck 2018).

3.3. Six Major Stages of Eclogite Xenolith Evolution

Sections 4 to 7, which review the contributions that the study of xenolithic eclogite can make to understanding terrestrial geodynamics through time, build on the paradigm that mantle-derived eclogites represent fragments of subducted oceanic crust. The evolution of xenolithic eclogites, from their formation in paleo-spreading ridges to their entrainment in the host magma, encompasses six major stages (**Figure 7**). Importantly, the associated processes do not equally affect the geochemical and isotopic parameters of a given xenolith, offering the possibility to extract information on various stages of eclogite evolution by targeting specific samples and proxies, as reviewed in the sections that follow. Fortunately, the large range of element abundances and isotope ratios that can now be determined by routine analyses makes it possible to accurately track the petrogenesis of each eclogite sample.

3.3.1 Formation at spreading ridges. Archean oceanic crustal sections plausibly had a stratigraphy similar to modern ones but were thicker due to higher melt fractions achieved below spreading ridges at higher T_P. The crust at modern oceanic spreading ridges consists of pillow lavas, flows, sheeted dike complexes, and gabbros, the latter constituting some 70% of crustal thickness (e.g., White & Klein 2014). Of nearly 1,000 xenolithic eclogites reviewed by Stachel et al. (2022), nearly 57% are recognized as gabbroic on the basis of bulk eclogite $Eu/Eu^* > 1.05$, comparable to modern oceanic crustal proportions. The difference may arise from changing conditions in the paleo-convecting mantle source (Section 5) and/or metasomatic alteration (Section 3.3.4). Plagioclase-rich cumulate protoliths for some or all samples in eclogite xenolith suites have long been recognized based on elevated CaO and Al_2O_3 contents, low and flat HREE patterns, and positive Eu and Sr anomalies (e.g., Neal et al. 1990, Jerde et al. 1993). Xenolithic eclogites with $Eu/Eu^* > 1.05$ in combination with low TiO_2 and ΣHREE abundances (HREEs only are summed to avoid effects of LREE loss due to melt depletion and gain due to metasomatic enrichment) have protoliths sampling the intrusive, gabbroic portion of oceanic crust but have overall highly variable element abundances similar to modern mid-ocean ridge gabbros (**Figure 1*a***). The complementary residual melts after cumulate crystallization develop negative Eu anomalies, which are recognized in basaltic eclogites with protoliths in the upper portion of oceanic crust, whereas samples without Eu anomalies have protoliths that experienced only minor plagioclase fractionation.

The successive crystallization of olivine, plagioclase, and clinopyroxene in dry peridotite-derived melts is characteristic for spreading ridges (e.g., Herzberg 2004). Some high-Mg eclogites may have originated as little-differentiated melts (i.e., only olivine ± plagioclase fractionation), whereas high-Ca eclogites are the result of advanced crystallization after clinopyroxene reached the liquidus, as evident from thermodynamic modeling of picrite crystallization (**Figure 6*b***). The

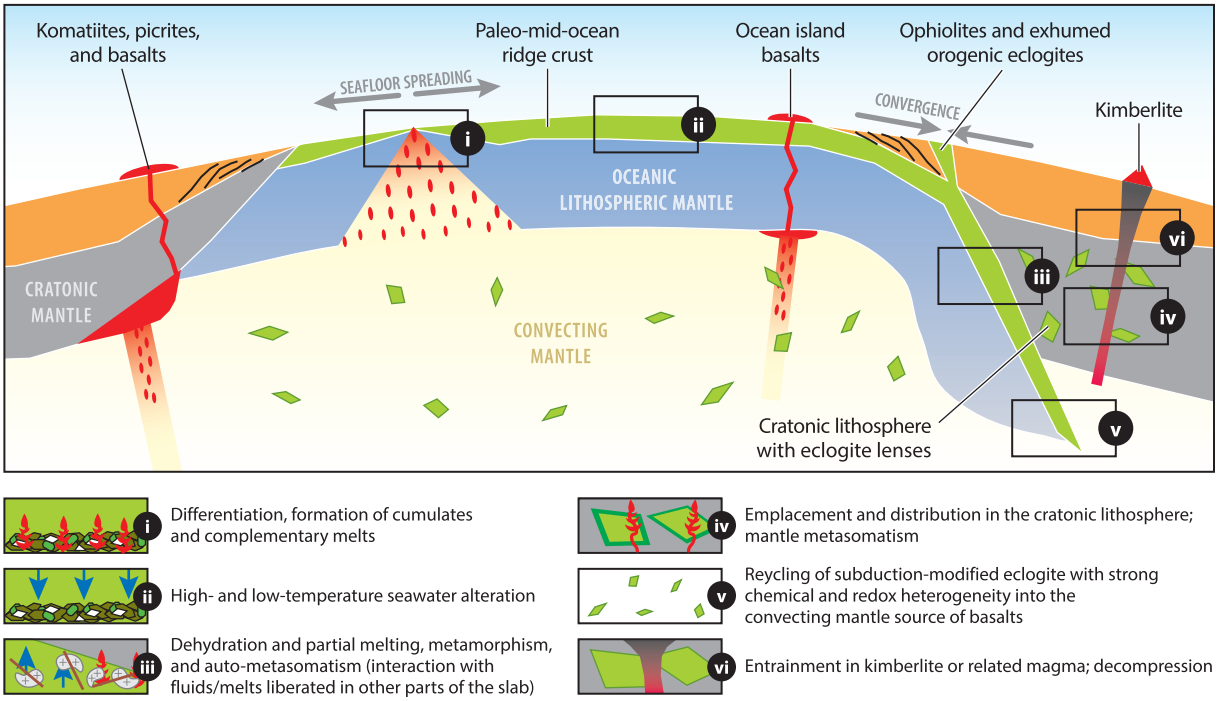

Figure 7

Illustration of the six major evolutionary stages of xenolithic eclogite and its low-pressure, oceanic crustal precursor in the Precambrian, when komatiite emplacement at continental margins was common but kimberlite magmatism was rare (e.g., Mole et al. 2014, Tappe et al. 2018). (*i*) Formation of cumulates and complementary melts by partial melting of warmer and potentially more reducing and partially depleted ambient mantle underlying paleo-spreading ridges. (*ii*) Alteration via interaction with O_2-poor, largely sulfate-free seawater producing fractionated stable isotope compositions, but having uncertain redox potential. (*iii*) Subduction along hotter temperature/pressure gradients and interaction of oceanic crust with fluids ± melts liberated by underlying serpentinized oceanic mantle and overlying sediments, as well as dehydration and partial melting of the oceanic crust itself. (*iv*) Emplacement of part of the subduction-modified eclogite residue in the cratonic lithospheric mantle, and exposure to metasomatic fluids and melts that sometimes form hydrous mineral-bearing eclogite, particularly in the shallow lithosphere, that may be detected as seismic discontinuities. (*v*) Recycling of some subduction-modified eclogite material into the convecting mantle where it contributes to compositional and redox heterogeneities in plume sources sampled, for example, by modern ocean island basalts. (*vi*) Entrainment of cratonic eclogite—typically billions of years after its emplacement into the lithosphere—in kimberlite and related rocks, and formation of a diverse suite of secondary minerals.

multitude of postformational processes affecting oceanic crust explains the considerable scatter in major and trace element compositions displayed by eclogites from individual localities and globally (**Figures 5*b*,*c***; **6*a*,*b***). In particular, most high-Mg eclogites are likely to have lost a partial melt, and many may have been metasomatized or interacted with peridotite, as discussed below.

3.3.2. Seawater alteration. The effects of seawater alteration are typically gauged by stable isotope compositions, which are readily fractionated at low temperatures pertaining to seawater alteration [up to ~400°C (Alt et al. 1986)] but undergo minimal fractionation at mantle temperatures (e.g., Kyser 2018). Since the recognition of a seawater alteration signature in xenolithic eclogites (Gregory & Taylor 1981), oxygen isotopes have been used for this purpose (e.g., Korolev et al. 2018) (**Figure 5*a***), but carbon and sulfur isotopes have also been employed (e.g., Deines et al. 1991; Burness et al. 2021, and references therein). The advent of highly sensitive and precise mass spectrometry techniques has also enabled detecting signatures of low-temperature fractionation

Supplemental Material >

Geothermobarometry and oxybarometry: application of experimentally calibrated thermometers and (oxy)barometers to retrieve the ambient temperature-pressure-oxygen fugacity conditions at which the eclogite equilibrated before kimberlite entrainment

in metal stable isotopes, such as Mg (e.g., Wang et al. 2015) and more recently Ca (Smart et al. 2021a) and Zn (Z.-Z. Wang et al. 2022) (**Supplemental Figure 2**). Variation in these nontraditional stable isotope systems is typically ascribed to seafloor weathering because mantle processes produce small or irresolvable isotope fractionations. Importantly, the absence of low-temperature fractionated stable isotope systems is not proof against a low-pressure origin because the degree of isotopic fractionation depends on the interplay of seawater availability and the temperature (and thus depth) of alteration, which at some oceanic crustal levels can result in $\delta^{18}O$ values indistinguishable from fresh MORB (Alt & Teagle 2003). Furthermore, some eclogite and pyroxenite xenoliths with protoliths derived from near the oceanic crust-mantle transition are unlikely to show seawater alteration signatures (Smart et al. 2012, Mikhailenko et al. 2021).

3.3.3. Subduction, metamorphism (eclogitization), and interaction with slab components. Most xenolithic eclogites record temperatures beyond those required for complete dehydration and wet partial melting of oceanic crust (**Figure 3*b***), such that eclogitized oceanic crust was probably dry and melt depleted postsubduction (see Section 5.1). Importantly, oceanic crust is overlain by sediment and underlain by variably hydrated oceanic mantle, which dehydrate and partially melt at different *P-T* conditions (e.g., Schmidt & Poli 2014). The diverse liberated fluids and melts may then interact with the oceanic crust within paleo-subduction zones and leave characteristic signatures (Aulbach et al. 2020) (see Section 5.2).

3.3.4. Emplacement and metasomatism in the cratonic lithospheric mantle. Although the mode of emplacement and retention of eclogitized oceanic crust in the cratonic lithosphere is uncertain (Section 6.1), geothermobarometry clearly locates xenolithic eclogites at depths above the lithosphere-asthenosphere boundary (**Figure 3*a***). The long delay between Archean to Paleoproterozoic emplacement of eclogite into the mantle lithosphere and generally Phanerozoic exhumation within kimberlite melts (**Supplemental Text**) provides a large time window for eclogite modification via interaction with metasomatic fluids and melts. Mantle metasomatism has been identified in xenolithic eclogites by disequilibrium textures and addition of volatile-bearing minerals, as well as mineral compositional heterogeneity, incompatible element enrichment, and zoning within minerals (e.g., Hills & Haggerty 1989, Ireland et al. 1994) (see **Supplemental Text**). Aulbach & Jacob (2016) used LREE enrichment expressed as normal mid-ocean ridge basalt (NMORB)-normalized Ce/Yb or Nd/Yb > 1 to identify metasomatized samples; however, melt-depleted samples may experience incompatible element enrichment yet retain sub-NMORB LREE/HREE, and MORB itself displays a wide range of Ce/Yb and Nb/Yb (e.g., compilation of Jenner & O'Neill 2012). It is therefore good practice to consider the entire REE pattern rather than just a ratio and check for additional signatures of metasomatism. Recognized widespread markers of metasomatism include an anticorrelation of MgO with FeO and positive correlation with SiO_2, particularly for xenoliths with >15 wt% MgO; these chemical changes are thought to be mediated by addition of a high-temperature pyroxene from kimberlite-like melts (Aulbach et al. 2020) (**Figure 6*b***). Because pyroxenite xenoliths with microstructures similar to xenolithic eclogites show many of the hallmarks of metasomatism, they can be considered an integral part of the evolution of eclogite sources in the lithospheric mantle. Importantly, intense mantle metasomatism can lead to a muting of crustal signatures, such as Eu/Eu^* approaching 1, a narrowing of $\delta^{18}O$ to mantle-like values (**Supplemental Figure 4**), and a reduction of garnet grossular content that in turn reduces the partitioning of incompatible elements into garnet (**Figure 1*c***; **Supplemental Text**). **Figure 6*c*** illustrates some of the secular compositional changes associated with mantle metasomatism, as inferred from the difference between bulk rocks reconstructed from inclusions

in diamond versus the weighted average of eclogite and pyroxenite xenoliths (Stachel et al. 2022).

3.3.5. Recycling of subduction-modified residues into the convecting mantle. Eclogite (or pyroxenite) that has been recycled into the convecting mantle is widely accepted to contribute to intraplate mafic magmatism, notably, to OIBs (e.g., Hofmann & White 1982, Stracke 2021). The importance of eclogite as a component in the convecting mantle becomes clear when considering the relatively small volume of eclogite (a few percent) stored in the subcontinental lithospheric mantle, which itself constitutes only some 1.5–2.5% of silicate Earth (McDonough 1991), versus eclogite that has been subducted through time (minimum 3% of the mass of silicate Earth) (Rudnick et al. 2000). OIBs sample mantle sources with average ages of ~1.8–2.0 Ga (e.g., Andersen et al. 2015). If these average ages have geological meaning, this implies that yet older (e.g., Archean) crustal material must have been recycled into the mantle, and there is ample evidence for Archean-aged eclogitic material hosted within the cratonic lithosphere (2.7–3.0 Ga eclogite dates) (**Figure 4**; **Supplemental Table 1**). Thus, xenolithic eclogites that have not been metasomatized subsequent to their emplacement in the continental lithosphere may be representative of the component inferred for some OIB sources, a topic that is discussed in Section 7.

Supplemental Material >

3.3.6. Exhumation with the host magma. Both xenolithic eclogites and some orogenic eclogites have MORB-like protoliths (Tsujimori & Mattinson 2021), but tectonic exhumation of orogenic eclogites occurs over Ma timescales (e.g., Kylander-Clark et al. 2012) compared to hours-to-days entrainment in kimberlite (e.g., Brett et al. 2015). Despite the short kimberlite entrainment time, infiltration of highly mobile kimberlite melt into xenoliths during decompression causes fracturing and xenolith disaggregation, leading to kelyphitic breakdown rims on garnet, especially if accompanied by heating (e.g., Pokhilenko 2021), and also formation of diopside-rich, spongy rims on primary clinopyroxene (e.g., Spetsius & Taylor 2002). The secondary mineral suite resulting from kimberlite magma percolation in veins within eclogite in response, or precursory, to entrainment is extensive and comprises, but is not limited to, amphibole, phlogopite, calcite, clinochlore, serpentine, djerfisherite, corundum, orthopyroxene, and K-feldspar (e.g., Mikhailenko et al. 2020). Conversely, kimberlite ascent is too fast to allow for significant compositional changes via volume diffusion, as attested by the relatively homogeneous compositions of minerals in xenolithic compared to orogenic eclogite, and Mg-Fe exchange thermometry locating them firmly in the mantle lithosphere (Jacob 2004).

4. PROBING THE PALEO-CONVECTING MANTLE WITH XENOLITHIC ECLOGITE

Considering that most xenolithic eclogite protoliths formed at oceanic spreading ridges (Section 3.2), the great value and potential of these samples is their ability to constrain physicochemical properties of the Precambrian ambient convecting mantle source from which their igneous protoliths formed (e.g., Foley 2011), analogous to how modern MORBs are used today (e.g., Kelley et al. 2006). Unlike fresh MORB, xenolithic eclogites were variably affected by secondary compositional modification (Section 3.4), and thus the crux and challenge with using xenolithic eclogites as proxies for mantle evolution in deep time are to identify elements that are relatively untouched by postformational processes and instead more accurately reflect the protolithic oceanic crust. The **Supplemental Text** informs on the rationale and approach to using xenolithic eclogites for insights into the nature of paleo-convecting mantle sources. That xenolithic eclogites can, with respect to certain variables, retain remarkably pristine information

despite Gyr-long mantle residence is demonstrated by the observation that gabbroic samples with plagioclase-rich protoliths retain geochemical and isotopic hallmarks of their origin as an ocean floor cumulate (**Figures 1*a*** and **4*b***).

4.1. Depletion of the Ambient Paleo-Convecting Mantle

Earth's linked petrological, geochemical, and dynamic evolution depends on the extent and timing of crust-mantle differentiation, accompanied by formation of a depleted mantle reservoir (e.g., Davies 2006). While modern oceanic crust is derived by partial melting of depleted, if mildly heterogeneous, convecting mantle source, it is unclear when the depleted mantle became established as a distinct and isotopically recognizable reservoir (e.g., Stracke 2012). Some eclogites with well-constrained ages (**Figure 4*a***) provide isotopic evidence for protolith derivation from a depleted mantle reservoir. Calculated initial $^{87}Sr/^{86}Sr$ for clinopyroxene in Paleoproterozoic and Mesoarchean eclogites from the Kaapvaal, Siberian, and Slave cratons are less radiogenic than values calculated for coeval primitive mantle (Aulbach & Arndt 2019a), indicating derivation from a depleted source with lower time-integrated Rb/Sr (**Figure 4*b***). The least radiogenic measured $^{87}Sr/^{86}Sr$ is typically retained in gabbroic eclogites with high Eu/Eu*, indicating a plagioclase-rich protolith. Thus, samples with a strong cumulate signature are prime targets for obtaining insights into the compositional evolution of the paleo-convecting mantle because, in contrast to basaltic eclogites, they evolved at very low Rb/Sr and can retain measured $^{87}Sr/^{86}Sr$ close to initial ratios. Furthermore, depleted initial $^{176}Hf/^{177}Hf$ has been measured in U-Pb dated zircons hosted within xenolithic eclogites from both the Arkhangelsk diamondiferous province [1.85 ± 0.04 Ga (Shchukina et al. 2018)] and the central Slave craton [2.1 ± 0.3 Ga (Schmidberger et al. 2007)]. Thus, the limited isotopic data for xenolithic eclogites suggest the presence of a depleted mantle reservoir from ca. 3 Ga, but further elucidation of mantle geochemical evolution rests on the availability of robust eclogite xenolith age constraints.

4.2. Temperature and Redox Evolution of the Ambient Paleo-Convecting Mantle

The evolution of mantle T_P is central to understanding Earth's dynamics and element cycles through time, due to the temperature effect on the rheology and melting relations of peridotite (e.g., Herzberg et al. 2010, Foley 2018) and on the loci and nature of metamorphic reactions in subduction zones (e.g., Schmidt & Poli 2014). The fO_2 of various mantle domains is an important intrinsic parameter because it affects the speciation of volatiles (e.g., reduced versus oxidized carbon and sulfur), which in turn controls the location of the mantle solidus and the composition and mobility of any resulting melts (e.g., Frost & McCammon 2008, Chowdhury & Dasgupta 2020). Unmetasomatized, noncumulate high-Mg Archean and Paleoproterozoic xenolithic eclogites with little-differentiated protoliths [i.e., those that experienced olivine and plagioclase fractionation only, when concentrations of mildly incompatible elements change little (**Supplemental Text**)] provide an opportunity to place constraints on T_P and fO_2 in deep geologic time, complementing estimates that exist based on models and selected (ultra)mafic magmas (e.g., Canil 1997, Davies 2008, Herzberg et al. 2010, Nicklas et al. 2019).

Using proxies (Al_2O_3, Ti, Sm) suggested to be immobile during partial melt extraction from eclogite (see discussion in Aulbach & Arndt 2019a,b) (**Figure 5*b,c***), two main lines of evidence suggest that high-Mg xenolithic eclogites record moderate T_P that is lower than the hottest model by some 100–150°C. First, they have Y and Al_2O_3 contents that are too high to reflect formation of the crustal protoliths via substantial partial melting of a garnet-bearing mantle source, qualitatively requiring intersection of the peridotite solidus at $P < \sim 3$ GPa. Second, when the abundances

Supplemental Material >

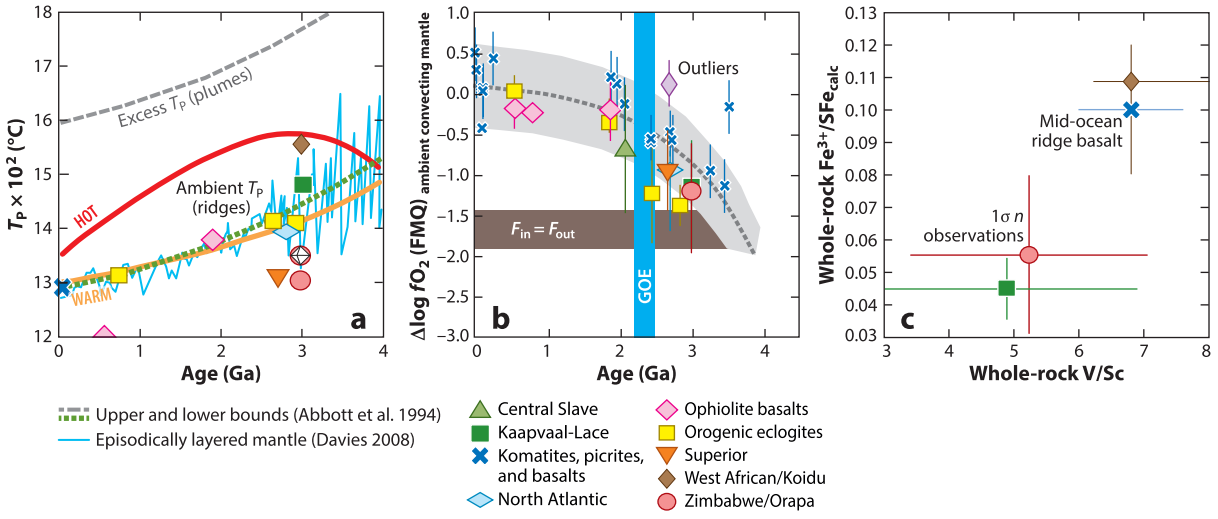

Figure 8

(*a*) Mantle potential temperature (T_P) as a function of age. Data points for individual xenolithic and orogenic eclogite suites are compared against various suggested T_P evolution curves for ambient and plume mantle (Aulbach & Arndt 2019b, and references therein) and a modeled curve for conditions of episodic mantle layering (Davies 2008). Only data for unmetasomatized noncumulate and little-differentiated (i.e., olivine ± plagioclase fractionation only) samples are used, of which 2–3 with the lowest TiO_2 content were chosen, which give the highest melt fraction (F) when inverted for the batch melting equation and, consequently, the highest T_P. Additional data points were obtained for the parental mid-ocean ridge basalt (MORB) estimate of Niu & O'Hara (2009), which yields T_P of 1,290°C, in agreement with warm temperature evolution curves for ambient mantle, and for bulk rocks reconstructed from eclogite xenoliths and from inclusions in eclogitic diamond from Orapa (*diamond in circle*) (data sources in Stachel et al. 2022). This illustrates the difference between eclogite xenoliths affected by mantle metasomatism versus inclusions protected by chemically inert diamond. (*b*) Oxygen fugacity (fO_2) of the ambient convecting mantle relative to the fayalite-magnetite-quartz (FMQ) buffer [in log units, $\Delta \log fO_2$ (FMQ)] as a function of age. Data points for individual xenolithic and orogenic eclogite suites, and for komatiite, picrite, and basalt lavas, the timing of the Great Oxidation Event (GOE), and fO_2 of the ambient convecting mantle are as in O'Neill & Aulbach (2022, and references therein); the stippled dark gray line and 1σ light gray envelope were estimated by fitting a trend to the eclogite and mafic lava data for gradual upward mixing of a deep early oxidized reservoir, excluding two outliers as marked in the figure. $F_{in} = F_{out}$ represents fO_2 conditions below which volcanic gases act as sinks and above which they act as sources of O_2 (Holland 2002). Panel adapted from O'Neill & Aulbach (2022) (CC BY 4.0). (*c*) Sympathetic behavior of V/Sc and $Fe^{3+}/\Sigma Fe$ in unmetasomatized eclogite and pyroxenite xenoliths from various localities. Panel adapted from Aulbach et al. (2019) (CC BY 4.0).

of incompatible elements, such as TiO_2 and Sm, are quantitatively inverted to obtain F using the batch melting equation, those fractions again indicate intersection of the peridotite solidus at relatively low P and therefore moderate T_P (details of the modeling in Aulbach & Arndt 2019a) (**Figure 8*a***). Gabbroic eclogites are Al_2O_3 rich and TiO_2 and Sm poor on account of their cumulate origin, and they are therefore unsuitable for this exercise. The current limited resolution of eclogite formation ages cannot detect short-term or regional changes in T_P related, for example, to mantle avalanches (e.g., Davies 2008). As discussed by Aulbach & Arndt (2019a), progress in constraining mantle T_P evolution is also crucial to the resolution of several related controversial issues, such as the viability of plate tectonics or the emergence of continents above sea level.

In the wake of core formation, the silicate convecting mantle would have been in equilibrium with metal and characterized by relatively low fO_2 [~$\Delta \log fO_2$ fayalite-magnetite-quartz (FMQ)-4.5] (Frost & McCammon 2008). The modern mantle has an fO_2 of around FMQ (as determined from $Fe^{3+}/\Sigma Fe$ of MORB glasses and from V distribution between olivine and calculated parental melts), and how and when the convecting mantle transitioned to more oxidized compositions remain a highly contentious issue (e.g., Nicklas et al. 2019, and references therein). The V redox

proxy holds its foundation in application to mantle-derived magmas (e.g., Canil 1997), and V is proposed to see through partial melt extraction from eclogite as confirmed by experiments (e.g., Holycross & Cottrell 2022). When V in xenolithic eclogites is ratioed over a homovalent element with similar behavior (here, Sc), the result implies that the Archean mantle was on average significantly (in the statistical sense) more reduced than younger mantle (O'Neill & Aulbach 2022). This is in accord with independent komatiite-derived data (Nicklas et al. 2019) (**Figure 8*b***) and also supported by $Fe^{3+}/\Sigma Fe$ in xenolithic eclogites (**Figure 8*c***), suggesting that $Fe^{3+}/\Sigma Fe$ is a more robust redox proxy than generally appreciated (Aulbach et al. 2019). In contrast to basaltic eclogites, gabbroic eclogites have low $Fe^{3+}/\Sigma Fe$ and V on account of their cumulate character and are therefore unsuitable to act as fO_2 proxies for the ancient mantle. If the mantle gradually became reoxidized across the Archean–Proterozoic boundaries, it would have had multiple implications, not least the liberation of more oxidized volcanic gases that helped bring about the Great Oxidation Event (Holland 2002) (**Figure 8*b***).

5. MODIFICATION OF ECLOGITE IN PALEO-SUBDUCTION ZONES

5.1. Eclogites as Markers of Plate Tectonic Processes and Formation of Archean Continental Crust

The mineralogy and composition of mantle xenolithic eclogites suggest loss of a partial melt, indicated by the absence of coesite/quartz in most samples, LREE-depleted compositions, and lower SiO_2 plus higher MgO contents compared to modern oceanic crust (e.g., Jacob 2004) (**Supplemental Figure 3**). As such, the dynamic significance of cratonic xenolithic eclogites was recognized early (Helmstaedt & Schulze 1989). Consequently, they were suggested and modeled as the complementary residues to extraction of a granitoid melt similar to TTGs (e.g., Ireland et al. 1994, Barth et al. 2001). Such modeling rests on extensive experimental constraints on amphibolite and eclogite phase relations, and robust trace element partitioning models at conditions relevant to subduction zones (e.g., Rapp & Watson 1995, Barth et al. 2002). Despite a convincing geochemical connection between TTGs and mantle eclogite, there exists a dearth of clearly temporally linked examples with the exception of ca. 2.7 Ga depleted xenolithic eclogites and overlying Neoarchean TTG complexes in West Greenland (Tappe et al. 2011). A similar connection was proposed for xenolithic eclogites and TTGs in West Africa (Rollinson 1997; Barth et al. 2001, 2002) and is possible within the very large uncertainty of the eclogite age determination. Thus, the xenolithic eclogite record does not support a prevalent complementary relationship between melt-depleted eclogite and TTG (**Figure 5**).

Supplemental Material >

An overarching conclusion that can be drawn from the subduction origin of eclogite within continental mantle is that ancient cratons formed during accretionary or collisional processes that have shaped continental evolution since the Mesoarchean (e.g., Helmstaedt & Schulze 1989, Tappe et al. 2011, Pearson & Wittig 2014). Diamonds containing eclogitic mineral inclusions have formation ages $\leq$3 Ga, possibly indicating the onset of plate tectonics (Shirey & Richardson 2011) and formation of eclogite during the consumption of ocean basins at convergent margins of cratonic nuclei (**Figure 7**). This is supported by a study of diamond from Mesoarchean sediments of the Witwatersrand, hence of bona fide antiquity, which show stable isotope characteristics requiring low-pressure processing at or near Earth's surface (Smart et al. 2016). It is conspicuous that eclogites on five cratons have Neo- to Mesoarchean ages [plus probably xenolithic eclogites from the West African craton, the ages of which remain ill-constrained (**Figure 4*a***)]. It is possible that these eclogites formed part of Earth's first supercontinent [Ur (Rogers & Santosh 2003)] and that they represent the first global, linked plate tectonic network. Orogenic eclogite suites

become rather common by the Paleoproterozoic (Tamblyn et al. 2021), and these ages are matched by eclogite xenolith suites from the Slave craton and the East European Platform (**Figure 4*a***), which plausibly formed part of the Nuna/Columbia supercontinent.

It has been suggested that, for density reasons, tectonically exhumed assemblages record hotter conditions than predicted and are typically returned from depths ≤80–100 km (Bebout 2014). Thus, the dominantly high peak temperature conditions experienced by pre–2 Ga exhumed metamorphic rocks (pink field in **Figure 3*b***) are bound to be unrepresentative. In this context, the value of xenolithic eclogites is that they may archive otherwise inaccessible information on the deeply subducted component at least in the early part of Earth's history.

5.2. Interaction of Paleo-Oceanic Crust with Other Slab Components and Volatile Cycling in Ancient Subduction Zones

Once sustained plate subduction became widespread on Earth, large-scale recycling of material that had interacted with the evolving atmosphere, hydrosphere, and nascent biosphere began. A suggested Archean subduction gradient (shown in **Figure 3*b***) lies at the hot end of the range of modern subduction zones, showing that postsubduction, most eclogites would be dry and possibly melt depleted. One question that might be addressed is when signatures similar to those produced in Phanerozoic subduction environments appear in the eclogite xenolith record. Exhumed Phanerozoic subduction terranes often show complex geochemical interactions between melts and fluids with the various lithologies contained within the subduction mélange (Bebout 2014). Comparably, some xenolithic eclogites show peculiar S-shaped or stepped REE patterns (Aulbach et al. 2020) (**Figure 9*a***), which resemble those produced in fluid transport systems in orogenic eclogites (John et al. 2004). These REE patterns may have resulted from the formation of new garnet accompanied by CaO enrichment during interaction with fluids derived from serpentinites, which are a major fluid source in subducting slabs (Beinlich et al. 2010) (**Figure 9*a***). Subducted sedimentary components have also been detected in xenolithic eclogites; interaction of Mesoarchean oceanic crust with pelite-derived melts is suggested based on the presence of highly radiogenic Sr ($^{87}Sr/^{86}Sr > 0.7080$) in some xenolithic eclogites combined with elevated Li abundances, which cannot be explained by metasomatism by kimberlite-like melts (**Figure 9*b***). They may instead reflect the deep subduction of sediments derived from the weathering of isotopically evolved continental crust, possibly in a setting similar to modern subduction mélanges (Viljoen et al. 1996, Aulbach et al. 2020). In this setting, some MgO-rich eclogites may also form in response to mingling and hybridization with peridotite (Smart et al. 2009, Korolev et al. 2021). In order to confidently recognize the signatures of interaction of paleo-oceanic crust with other slab components, stable Li and B isotope compositions, which are highly mobile elements with distinctive ratios in mantle and crustal reservoirs, could be employed (Marschall et al. 2017). In addition, Mg and Zn isotope measurements have been applied to xenolithic eclogites (e.g., Wang et al. 2015, Z.-Z. Wang et al. 2022) and show promise as sensors for the presence of oxidized carbon in ancient subduction zones.

At the same time, fO_2 constraints suggest that graphite or diamond is generally the stable carbon mineral in xenolithic eclogites and additionally require that any oxidized S species would have been reduced to sulfide (**Figure 3*c***). Xenolithic eclogites do not contain primary carbonate or sulfate, but they are frequently graphite/diamond and sulfide rich, including sulfides with heavy $\delta^{34}S$ that may have formed via reduction of sedimentary sulfate (e.g., Burness et al. 2020, 2021) (**Figure 5*a***). It is noteworthy that sulfide inclusions in diamond are overabundant with respect to mantle S contents (Stachel & Harris 2008), and a portion of both eclogite diamond and its sulfide inclusions have non-mantle C and S isotopes (Cartigny et al. 2014, and references therein). This

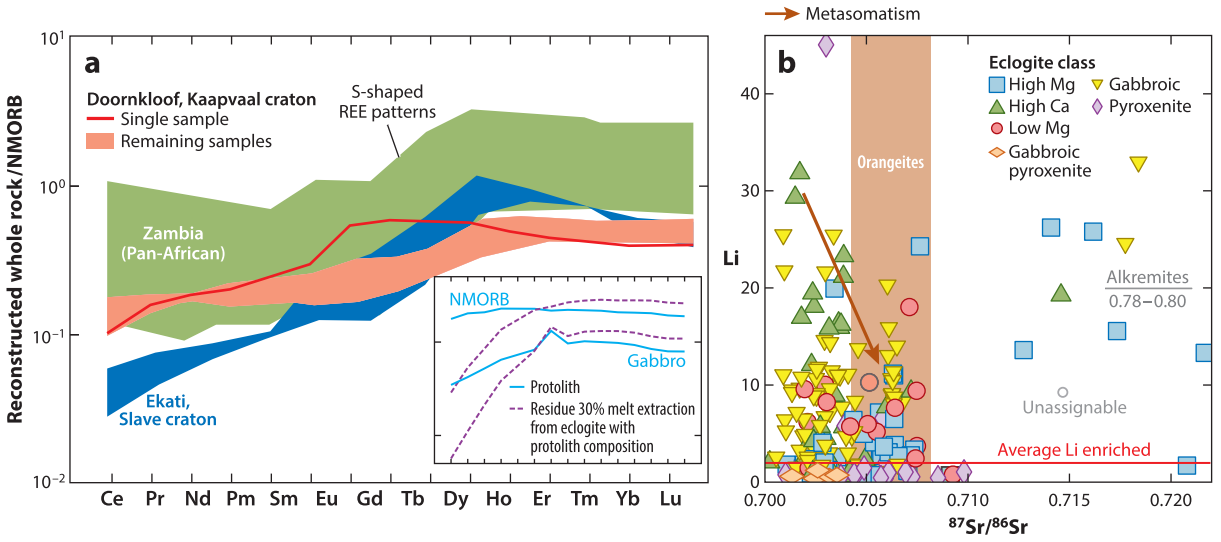

Figure 9

(*a*) S-shaped, stepped rare earth element (REE) patterns or middle rare earth element (MREE)-depleted patterns of bulk eclogite and pyroxenite xenoliths from Ekati on the central Slave craton and from Doornkloof on the Kaapvaal craton (data sources in **Supplemental Table 1**). Shown for comparison are similar REE patterns in orogenic eclogites from Zambia that cannot be generated during partial melting but instead result from eclogite facies fluid-rock interaction at high fluxes (John et al. 2004). The inset in panel *a* shows modeled composition for extraction of 30% partial melt from eclogite with normal mid-ocean ridge basalt (NMORB) or mid-ocean ridge (MOR) gabbro composition (modeling parameters in Aulbach & Jacob 2016), illustrating that partial melt extraction cannot generate S-shaped patterns with MREE depletion. (*b*) $^{87}Sr/^{86}Sr$ versus Li abundances (μg/g) in clinopyroxene from eclogite and pyroxenite xenoliths from various localities (data sources in **Supplemental Table 1**). Values for alkremites linked to subducted sediments exceed the scale (Mazzone & Haggerty 1989). The range for orangeites (a Kaapvaal craton–specific term for lamproite) from isotopically aged lithospheric sources in the Kaapvaal craton (Becker & le Roex 2006) is shown for comparison. Mantle metasomatism (*brown arrow*) strongly reduces Li abundances [*horizontal red line* shows average Li abundance for enriched eclogite xenoliths by Aulbach et al. (2020)]; therefore, the association of radiogenic Sr with high Li abundances may point to interaction with crustal fluids or melts rather than interaction with kimberlite-like melts.

Supplemental Material >

highlights carbon-sulfur [±Fe (Jacob et al. 2016)] redox interactions in ancient subduction zones and suggests deep C-S recycling, despite expectations according to some estimates that very little carbon is recycled past subarc depths, at least for modern subduction zones (Kelemen & Manning 2015).

6. ECLOGITE AS A COMPONENT IN THE CRATONIC LITHOSPHERIC MANTLE

6.1. How Is Paleo-Oceanic Crust Emplaced in the Cratonic Lithosphere?

Only a small portion of oceanic crust subducted through time (Rudnick et al. 2000) has been captured in the lithospheric mantle, where it forms a volumetrically minor but geochemically and mineralogically important component (e.g., Garber et al. 2018) (**Supplemental Text**). The wide distribution of eclogite in the lithosphere column (**Figure 3*a***) may be indicative of eclogite occurrence as pods and lenses after disruption of oceanic plates. Luo & Korenaga (2020) address the problem of the mass imbalance, which arises from a model of craton construction from imbricated plates versus the observed abundance of eclogite in the lithospheric mantle, and employ numerical modeling to argue that prior to 3 Ga, eclogite would have been completely purged from the lithosphere. Conversely, the modeling of Z. Wang et al. (2022) suggests that eclogite need not

be completely lost from the lithosphere and that viscous drainage leads to a redistribution of this material, consistent with observations.

6.2. Cratonic Eclogite as Part of the Lithosphere's Diamond and Metal Endowment

The significance of eclogite as a diamond source rock becomes evident considering its scarcity in the continental lithosphere (few volume percent) against the observation that some 33% of inclusion-bearing diamonds (the inclusions allowing relatively accurate assignment to source lithology) are eclogitic (Stachel & Harris 2008). The dominantly low fO_2 determined for xenolithic eclogites, in agreement with the generally reducing nature of the continental lithospheric mantle (Foley 2011), is below the water maximum for CHO fluids (**Figure 3*c***), which causes efficient reduction of oxidized carbon present within fluids released from different reservoirs in the down-going slab (Aulbach et al. 2019). Diamond formation in eclogite due to reduction of relatively oxidized fluids is suggested from carbon isotope constraints (e.g., Smart et al. 2012), the inferred presence of recycled sulfate (Burness et al. 2021), and carbonatitic microfluid inclusions in diamond (e.g., Weiss et al. 2022), as well as the geochemical signatures borne by host eclogites that indicate metasomatism by carbonatitic media (Smart et al. 2009, Mikhailenko et al. 2020). Conversely, in some eclogite suites, oxidation of methane-dominated hydrous fluids may have facilitated diamond formation (e.g., Smart et al. 2017, Smit et al. 2019). Finally, redox-neutral formation from mixed CO_2-CH_4-bearing fluids near the H_2O maximum may be important (Stachel et al. 2022).

While the role of the lithospheric mantle in crustal ore body metallogenesis is contentious (Arndt 2013, Griffin et al. 2013), recent investigations into the highly siderophile element (HSE) geochemistry of platinum group element (PGE)-bearing base metal sulfides and other platinum group minerals found within xenolithic eclogite, as well as inclusions within eclogitic diamonds, have highlighted the capacity of mantle eclogite to serve as a viable source rock for magmatic sulfide deposits. Base metal sulfides and platinum group minerals occur only in trace amounts ($\ll$1 vol%) within mantle eclogite and are generally characterized by lower PGE concentrations and more variable $\delta^{34}S$ values (from -11 to $+29$‰) than peridotite (e.g., Burness et al. 2021, Hughes et al. 2021), although some eclogitic sulfides with elevated HSE contents have been related to mantle metasomatism (Burness et al. 2020). A link between mantle eclogite and magmatic ore body formation has been suggested, particularly for the 2.05 Ga Bushveld complex of the Kaapvaal craton based on comparison of Sr and Os isotopic compositions for Kaapvaal mantle eclogite and Bushveld PGE-bearing lithologies (Richardson & Shirey 2008, Wilson et al. 2017). Integration of eclogite HSE contents into mantle melting models has demonstrated that PGE-bearing melts derived from Kaapvaal eclogites can reproduce the composition of parental melts for the Bushveld orebody layers (Hughes et al. 2021), providing more quantitative evidence that lithospheric eclogite contributes to the metal endowment of crustal magmatic ore bodies.

6.3. Geophysical Properties of the Mantle Eclogite Source

Recent work has demonstrated that eclogite significantly contributes to the lithospheric mantle's electrical conductivity, gravity, and seismic velocity signature (Garber et al. 2018). Based on average eclogite compositions, the presence of up to 20 vol% eclogite and 2% diamond can alleviate the problem of the bulk seismic velocity of the lithospheric mantle markedly exceeding that of peridotite, while not violating bulk lithosphere gravity constraints related to the greater density of eclogite (Garber et al. 2018). Subsequently, the density and seismic velocity have been assessed for reported compositions of individual mantle eclogite suites from multiple cratons, with the finding that mantle metasomatism, through its reduction of FeO content, reduces

eclogite density and hence enhances its gravitational stability, while having negligible effects on shear-wave velocity (Aulbach et al. 2020). Moreover, for moderate abundances of eclogite in the continental lithosphere (~1 vol%), thermal effects are not expected, as low contents of heat-producing elements in eclogite correspond to a heat generation of just 0.006 $\mu W/m^3$, compared to 0.00004 $\mu W/m^3$ for unmetasomatized depleted peridotite and on par with 0.006 $\mu W/m^3$ for metasomatized peridotite (McIntyre et al. 2021). However, this issue may need to be revisited considering the markedly higher eclogite abundance suggested by Garber et al. (2018).

As clinopyroxene accommodates appreciable amounts of H_2O [up to almost 1,000 wt% ppm (e.g., Katayama et al. 2006)], oceanic crust transformed to eclogite with some 50% clinopyroxene not only can entrain significant amounts of water into the deep convecting mantle but also contributes to the bulk magnetotelluric signature of the continental lithosphere (e.g., Huang et al. 2014, Radu et al. 2022). However, eclogite H_2O contents and their effects on conductivity remain poorly constrained yet are critical for accurate interpretations of the cratonic lithosphere's magnetotelluric signatures.

Mid-lithospheric discontinuities (MLDs), which are generated by strong negative gradients in seismic velocities at 60–160 km depth, have been detected widely in continental lithosphere, which can be explained by the metasomatic introduction of seismically slow hydrous minerals, such as amphibole and phlogopite (Rader et al. 2015). As mantle metasomatism in eclogite is typically concentrated in this depth interval, a link to MLDs was suggested (Aulbach et al. 2020). A rare suite of amphibole-bearing xenolithic eclogites from Palmietfontein (Kaapvaal craton) could be linked to Mesozoic metasomatism by kimberlites based on Pb isotopic constraints, and their relatively shallow depth of derivation was shown to overlap a regionally detected MLD (Smart et al. 2021b).

7. ECLOGITE AS A DISCRETE MANTLE COMPONENT IN THE CONVECTING MANTLE

A fundamental paradigm in mantle geochemistry is that the spread in incompatible element and radiogenic isotopic compositions of OIBs and also some MORBs is a result of the contribution of recycled crustal materials to basaltic magmatism (e.g., Hofmann & White 1982, Stracke 2021). Because this recycled material has an average age of ~2 Ga (Andersen et al. 2015), it may well be represented by Archean to Paleoproterozoic xenolithic eclogite (Section 2), keeping in mind that metasomatized eclogites are unsuitable because they acquired their chemical characteristics during postsubduction residence in the cratonic lithosphere (Section 3.4). The crustal end member materials, now existing as eclogite or pyroxenite in the mantle, are generally represented by modeled compositions of subduction-modified oceanic crust (e.g., Lambart et al. 2016), rather than actual eclogite compositions. This may also reflect the paucity of radiogenic and stable isotopic data for mantle-derived eclogites that could be used in modeling, with few exceptions (e.g., Jacob et al. 2005).

Recent application of nontraditional metal stable isotopes (e.g., Ca-Fe-Mg-Zn) to oceanic basalts and mantle-derived eclogites provides new opportunities for interrogating the contributions of recycled crustal components to oceanic magmatism because these time-independent systems are not based on incompatible elements susceptible to metasomatic overprinting (e.g., Soderman et al. 2022). The presence of garnet-rich eclogite (or pyroxenite) will impose nontrivial stable isotope fractionation during partial melting, particularly for ^{26}Mg and ^{44}Ca (e.g., Soderman et al. 2022). Indeed, many OIBs and MORBs have Fe, Mg, and Ca stable isotope signatures that are fractionated by only a few 0.1‰ and, thus, can be accounted for by partial melting of mantle peridotite (e.g., Soderman et al. 2022). However, some OIBs (e.g., Stracke et al. 2018, Nebel et al. 2019) require sources with markedly fractionated stable isotopic compositions that clearly exist in the burgeoning eclogite rock record: Ca-Mg-Zn stable isotopic compositions of mantle-derived

eclogites overlap with, but are also fractionated from, the known mantle compositional range (e.g., Wang et al. 2015, Smart et al. 2021a, Z.-Z. Wang et al. 2022), similar to the mantle eclogite $\delta^{18}O$ record (Korolev et al. 2018). More systematic and comprehensive studies of the isotope compositions of eclogites globally are needed to fully appreciate the contribution of eclogite to heterogeneity in the convecting mantle and its role as a repository of missing elements and isotopes in the global mass balance (with respect to a bulk Earth model).

SUMMARY POINTS

1. Mantle-derived xenolithic eclogites represent recycled fragments of Mesoarchean to Paleoproterozoic oceanic crust and have a multistep petrogenesis that includes formation as oceanic basalts and gabbros at spreading ridges, near-surface seawater and hydrothermal fluid alteration, metamorphism in subduction channels attended by fluid and melt loss, recycling of the dominant proportion into the convecting mantle, emplacement of a subportion within the cratonic lithosphere followed by variable mantle metasomatism, and finally entrainment in the transporting magma (e.g., kimberlite) to Earth's surface. Each step of eclogite petrogenesis informs geoscientists about the physical and chemical conditions of deep geochemical cycles associated with the generation of mantle-derived melts and subduction tectonics.
2. Archean oceanic crust, now xenolithic eclogites, had geochemical and isotopic compositions that indicate the contemporaneous ambient convecting mantle was at least in parts geochemically depleted by 3 Ga and was only moderately hotter (by 100–150°C) but more reduced (by 1–1.5 log units) than the modern convecting mantle.
3. Xenolithic eclogite retains O-S-Ca-Mg-Zn stable isotope signatures that can be inherited only from low-temperature processes as part of the oceanic lithosphere; in combination with enriched geochemical and isotopic compositions relative to peridotite, compositions of unmetasomatized mantle eclogites are representative end members to explain the enriched trace element and isotopic characteristics of some ocean island basalt and mid-ocean ridge basalt sources, and, when fully characterized, may help alleviate some long-standing terrestrial mass balance problems.
4. Isotopic and trace element constraints suggest that processing of paleo-oceanic crust in subduction zones involved partial melt loss and interaction with other portions of the slab, specifically sediments and serpentinites. This may indicate that mélange-type settings have characterized some subduction zones since ca. 3.0–2.7 Ga, a time when eclogite emplacement into the cratonic lithosphere of at least five cratons marks closure of ocean basins during craton amalgamation, possibly related to their coalescence into Earth's first supercontinent. Conversely, despite a compositional complementarity of residual eclogite and tonalite-trondhjemite-granodiorite, a temporal link is not strongly indicated.
5. Although eclogite is a subordinate lithology in cratonic mantle, its contribution to gravity, seismic velocity, and conductivity signatures of the bulk cratonic lithosphere is significant due to its typically greater density and seismic velocity, and also the fact that it is a dominant host for diamond, which itself has geophysical impacts beyond its small proportion, as well as the capacity of eclogite to accommodate hundreds to thousands weight percent parts per million H_2O, in particular within clinopyroxene. Moreover,

metasomatic signatures in xenolithic eclogites prevail for relatively shallow residence depths, where mid-lithospheric discontinuities are seismically detected.

6. Xenolithic eclogite plays an important role in the mineral endowment of cratons, hosting a disproportionate portion of diamond compared to its abundance in the lithosphere. Investigations of platinum group element budgets of mantle eclogites show that, while levels of highly siderophile element abundances in eclogite-hosted sulfides are low, moderate-degree melting events can effectively mobilize chalcophile elements into S-bearing melts that may be involved in crustal orthomagmatic ore deposits.

FUTURE ISSUES

1. It is widely accepted that mantle xenolithic eclogites represent ancient oceanic crust that was subducted and captured into lithospheric mantle. While recent numerical modeling studies have begun to address this issue, the detailed dynamics of eclogite emplacement, retention, and ultimate distribution in the lithosphere are not yet fully understood.
2. Detailed mineralogical and chemical similarities and differences between Mesoarchean to Paleoproterozoic xenolithic eclogites and predominantly younger orogenic eclogites have yet to be systematically investigated; disparities may reflect differences in the physicochemical conditions at which their protoliths formed and, for similarly aged xenolithic and orogenic eclogites, may uncover different physicochemical conditions under which oceanic crust is either exhumed or deeply subducted.
3. Reliable barometry and dating for typically high-variance eclogite systems remain elusive. Novel machine-learning approaches, such as applied to majorite barometry (Thomson et al. 2021), and application of single-mineral Sm-Nd and Rb-Sr geochronology afforded by ultrasensitive instruments (Koornneef et al. 2014) to inclusions in diamond or garnet that are least likely to be affected by disturbance of the radiogenic isotope system and parent-daughter ratios may alleviate this problem.
4. Stable isotope studies (e.g., Li, B, Mg, Ca, Fe) will prove useful in the quest to characterize fluid- and melt-related processes as well as fingerprint participating lithologies within ancient subduction zone systems.
5. A systematic characterization of novel stable isotopes will also allow better documentation of subducted oceanic crust in the convecting mantle as sampled by intraplate basalts and assessment of the role of eclogite in global elemental and isotopic mass balances.
6. Given that oxygen fugacity (fO_2) estimates for xenolithic eclogites cover a range where variations in the speciation of multivalent elements would be expected (**Figure 4**), experiments are needed to fully map out Eu-V-Cr partitioning specifically between eclogite minerals and melt as a function of fO_2, which may ultimately allow use of the distribution of these elements as redox sensors of metamorphic processes.
7. A better understanding is needed to determine under what conditions refractory eclogite that already experienced early dehydration melting can melt again, either during subduction when infiltrated by slab-derived fluids or as part of heterogeneous upwelling mantle packages, where its remelting and interaction of the melt with peridotite are often inferred.

DISCLOSURE STATEMENT

The authors are not aware of any affiliations, memberships, funding, or financial holdings that might be perceived as affecting the objectivity of this review.

ACKNOWLEDGMENTS

We are grateful to the *Annual Review of Earth and Planetary Sciences* Editorial Committee for the invitation to contribute. This project was funded by the Deutsche Forschungsgemeinschaft (DFG, German Research Foundation), project AU356/12 to S.A. K.A.S. acknowledges the support of the University of Tromsø Universitetsbiblioteket.

LITERATURE CITED

Abbott D, Burgess L, Longhi J, Smith WHF. 1994. An empirical thermal history of the Earth's upper mantle. *J. Geophys. Res.* 99(B7):13835–50

Alt JC, Muehlenbachs K, Honnorez J. 1986. An oxygen isotopic profile through the upper kilometer of the oceanic crust, DSDP Hole 504B. *Earth Planet. Sci. Lett.* 80:217–29

Alt JC, Teagle DAH. 2003. Hydrothermal alteration of upper oceanic crust formed at a fast-spreading ridge: mineral, chemical, and isotopic evidence from ODP Site 801. *Chem. Geol.* 201:191–211

Alvaro M, Mazzucchelli ML, Angel RJ, Murri M, Campomenosi N, et al. 2020. Fossil subduction recorded by quartz from the coesite stability field. *Geology* 48:24–28

Andersen MB, Elliott T, Freymuth H, Sims KWW, Niu Y, Kelley KA. 2015. The terrestrial uranium isotope cycle. *Nature* 517:356–59

Arndt NT. 2013. The lithospheric mantle plays no active role in the formation of orthomagmatic ore deposits. *Econ. Geol.* 8:1953–70

Artemieva IM. 2006. Global 1° × 1° thermal model TC1 for the continental lithosphere: implications for lithosphere secular evolution. *Tectonophysics* 416:245–77

Asimow PD. 2022. The petrological consequences of the estimated oxidation state of primitive MORB glass. In *Magma Redox Geochemistry*, ed. R Moretti, DR Neuville, pp. 139–54. Hoboken, NJ: Wiley & Sons

Aulbach S, Arndt NT. 2019a. Eclogites as palaeodynamic archives: evidence for warm (not hot) and depleted (but heterogeneous) Archaean ambient mantle. *Earth Planet. Sci. Lett.* 505:162–72

Aulbach S, Arndt NT. 2019b. Origin of high-Mg bimineralic eclogite xenoliths in kimberlite: reply to comment from Claude Herzberg. *Earth Planet. Sci. Lett.* 510:234–37

Aulbach S, Jacob DE. 2016. Major- and trace-elements in cratonic mantle eclogites and pyroxenites reveal heterogeneous sources and metamorphic processing of low-pressure protoliths. *Lithos* 262:586–605

Aulbach S, Massuyeau M, Garber JM, Gerdes A, Heaman LM, Viljoen KS. 2020. Ultramafic carbonated melt- and auto-metasomatism in mantle eclogites: compositional effects and geophysical consequences. *Geochem. Geophys. Geosyst.* 21:e2019GC008774

Aulbach S, Pearson NJ, O'Reilly SY, Doyle BJ. 2007. Origins of xenolithic eclogites and pyroxenites from the Central Slave Craton, Canada. *J. Petrol.* 48:1843–73

Aulbach S, Woodland AB, Stagno V, Korsakov AV, Mikhailenko D, Golovin A. 2022. Fe^{3+} distribution and $Fe^{3+}/\Sigma Fe$-oxygen fugacity variations in eclogite xenoliths, with comments on clinopyroxene-garnet oxy-thermobarometry. *J. Petrol.* 63(8):egac07

Aulbach S, Woodland AB, Stern RA, Vasilyev P, Heaman LM, Viljoen KS. 2019. Evidence for a dominantly reducing Archaean ambient mantle from two redox proxies, and low oxygen fugacity of deeply subducted oceanic crust. *Sci. Rep.* 9:20190

Barth MG, Foley SF, Horn I. 2002. Partial melting in Archean subduction zones: constraints from experimentally determined trace element partition coefficients between eclogitic minerals and tonalitic melts under upper mantle conditions. *Precambrian Res.* 113:323–40

Barth MG, Rudnick RL, Horn I, McDonough WF, Spicuzza MJ, et al. 2001. Geochemistry of xenolithic eclogites from West Africa, part I: a link between low MgO eclogites and Archean crust formation. *Geochim. Cosmochim. Acta* 65:1499–527

Bebout GE. 2014. Chemical and isotopic cycling in subduction zones. See Holland et al. 2014, pp. 703–47
Becker M, Le Roex AP. 2006. Geochemistry of South African on- and off-craton, Group I and Group II kimberlites: petrogenesis and source region evolution. *J. Petrol.* 47:673–703
Beinlich A, Klemd R, John T, Gao J. 2010. Trace-element mobilization during Ca-metasomatism along a major fluid conduit: eclogitization of blueschist as a consequence of fluid–rock interaction. *Geochim. Cosmochim. Acta* 74:1892–922
Bolhar R, Hofmann A, Kemp AIS, Whitehouse MJ, Wind S, Kamber BS. 2017. Juvenile crust formation in the Zimbabwe Craton deduced from the O-Hf isotopic record of 3.8–3.1 Ga detrital zircons. *Geochim. Cosmochim. Acta* 215:432–46
Brett RC, Russell JK, Andrews GDM, Jones TJ. 2015. The ascent of kimberlite: insights from olivine. *Earth Planet. Sci. Lett.* 424:119–31
Brown M, Johnson T. 2019. Metamorphism and the evolution of subduction on Earth. *Am. Mineral.* 104:1065–82
Burness S, Smart KA, Tappe S, Stevens G, Woodland AB, Cano E. 2020. Sulphur-rich mantle metasomatism of Kaapvaal craton eclogites and its role in redox-controlled platinum group element mobility. *Chem. Geol.* 542:119476
Burness S, Thomassot E, Smart KA, Tappe S. 2021. Sulphur isotopes (δ34S and Δ33S) in sulphides from cratonic mantle eclogites: a glimpse of volatile cycling in ancient subduction zones. *Earth Planet. Sci. Lett.* 572:117118
Canil D. 1997. Vanadium partitioning and the oxidation state of Archaean komatiite magmas. *Nature* 389:842–45
Cartigny P, Palot M, Thomassot E, Harris JW. 2014. Diamond formation: a stable isotope perspective. *Annu. Rev. Earth Planet. Sci.* 42:699–732
Chin EJ. 2018. Deep crustal cumulates reflect patterns of continental rift volcanism beneath Tanzania. *Contrib. Mineral. Petrol.* 173:85
Chowdhury P, Dasgupta R. 2020. Sulfur extraction via carbonated melts from sulfide-bearing mantle lithologies—implications for deep sulfur cycle and mantle redox. *Geochim. Cosmochim. Acta* 269:376–97
Czas J, Stachel T, Pearson DG, Stern RA, Read GH. 2018. Diamond brecciation and annealing accompanying major metasomatism in eclogite xenoliths from the Sask Craton, Canada. *Mineral. Petrol.* 112:311–23
Dasgupta R. 2013. Ingassing, storage, and outgassing of terrestrial carbon through geologic time. *Rev. Mineral. Geochem.* 75:183–229
Davies GF. 2006. Gravitational depletion of the early Earth's upper mantle and the viability of early plate tectonics. *Earth Planet. Sci. Lett.* 243:376–82
Davies GF. 2008. Episodic layering of the early mantle by the 'basalt barrier' mechanism. *Earth Planet. Sci. Lett.* 275:382–92
Day HW. 2012. A revised diamond-graphite transition curve. *Am. Mineral.* 97:52–62
de Oliveira Chaves A. 2021. Columbia (Nuna) supercontinent with external subduction girdle and concentric accretionary, collisional and intracontinental orogens permeated by large igneous provinces and rifts. *Precambrian Res.* 352:106017
Deines P, Harris JW, Robinson DN, Gurney JJ, Shee SR. 1991. Carbon and oxygen isotope variations in diamond and graphite eclogites from Orapa, Botswana, and the nitrogen-content of their diamonds. *Geochim. Cosmochim. Acta* 55:515–24
Evans KA, Tomkins AG. 2011. The relationship between subduction zone redox budget and arc magma fertility. *Earth Planet. Sci. Lett.* 308:401–9
Foley BJ. 2018. The dependence of planetary tectonics on mantle thermal state: applications to early Earth evolution. *Philos. Trans. R. Soc. A* 376:20170409
Foley SF. 2011. A reappraisal of redox melting in the Earth's mantle as a function of tectonic setting and time. *J. Petrol.* 52:1363–91
Frost DJ, McCammon CA. 2008. The redox state of Earth's mantle. *Annu. Rev. Earth Planet. Sci.* 36:389–420
Gale A, Dalton CA, Langmuir CH, Su YJ, Schilling JG. 2013. The mean composition of ocean ridge basalts. *Geochem. Geophys. Geosyst.* 14:489–518
Garber JM, Maurya S, Hernandez JA, Duncan MS, Zeng L, et al. 2018. Multidisciplinary constraints on the abundance of diamond and eclogite in the cratonic lithosphere. *Geochem. Geophys. Geosyst.* 19:2062–86

Ghiorso MS, Hirschmann MM, Reiners PW, Kress VC. 2002. The pMELTS: a revision of MELTS for improved calculation of phase relations and major element partitioning related to partial melting of the mantle to 3 GPa. *Geochem. Geophys. Geosyst.* 3:1–35

Gregory RT, Taylor HP. 1981. An oxygen isotope profile in a section of cretaceous oceanic crust, Samail ophiolite, Oman—evidence for $\delta^{18}O$ buffering of the oceans by deep (>5 km) seawater-hydrothermal circulation at mid-ocean ridges. *J. Geophys. Res.* 86(B4):2737–55

Griffin WL, Begg GC, O'Reilly SY. 2013. Continental-root control on the genesis of magmatic ore deposits. *Nat. Geosci.* 6:905–10

Griffin WL, Belousova EA, O'Neill C, O'Reilly SY, Malkovets V, et al. 2014. The world turns over: Hadean–Archean crust–mantle evolution. *Lithos* 189:2–15

Gurney JJ, Helmstaedt HH, Richardson SH, Shirey SB. 2010. Diamonds through time. *Econ. Geol.* 105:689–712

Hasterok D, Chapman DS. 2011. Heat production and geotherms for the continental lithosphere. *Earth Planet. Sci. Lett.* 307:59–70

Helmstaedt H, Schulze DJ. 1989. Southern African kimberlites and their mantle sample: implications for Archean tectonics and lithosphere evolution. In *Evolution and Differentiation of the Continental Crust*, ed. R Rushmer, pp. 67–91. Cambridge, UK: Cambridge Univ. Press

Helmstaedt HH, Pehrsson SJ. 2012. Geology and tectonic evolution of the Slave Province—a post-Lithoprobe perspective. In *Tectonic Styles in Canada: The Lithoprobe Perspective*, ed. JA Percival, FA Cook, RM Clowes, pp. 379–466. Newfoundland, Can.: Geol. Assoc. Can.

Herzberg C. 2004. Partial crystallization of mid-ocean ridge basalts in the crust and mantle. *J. Petrol.* 45:2389–405

Herzberg C, Condie K, Korenaga J. 2010. Thermal history of the Earth and its petrological expression. *Earth Planet. Sci. Lett.* 292:79–88

Hills DV, Haggerty SE. 1989. Petrochemistry of eclogites from the Koidu Kimberlite Complex, Sierra-Leone. *Contrib. Mineral. Petrol.* 103:397–422

Hofmann AW, White WM. 1982. Mantle plumes from ancient oceanic crust. *Earth Planet. Sci. Lett.* 57:421–36

Holland HD. 2002. Volcanic gases, black smokers, and the Great Oxidation Event. *Geochim. Cosmochim. Acta* 66:3811–26

Holland HD, Turekian KK, Rudnick RL, eds. 2014. *The Crust.* Amsterdam: Elsevier/Pergamon, 2nd ed.

Holycross M, Cottrell E. 2022. Experimental quantification of vanadium partitioning between eclogitic minerals (garnet, clinopyroxene, rutile) and silicate melt as a function of temperature and oxygen fugacity. *Contrib. Mineral. Petrol.* 177:21

Huang JX, Li P, Griffin WL, Xia QK, Gréau Y, et al. 2014. Water contents of Roberts Victor xenolithic eclogites: primary and metasomatic controls. *Contrib. Mineral. Petrol.* 168:1092

Hughes HSR, Compton-Jones C, McDonald I, Kiseeva ES, Kamenetsky VS, et al. 2021. Base metal sulphide geochemistry of southern African mantle eclogites (Roberts Victor): implications for cratonic mafic magmatism and metallogenesis. *Lithos* 382–383:105918

Ireland TR, Rudnick RL, Spetsius Z. 1994. Trace elements in diamond inclusions from eclogites reveal link to Archean granites. *Earth Planet. Sci. Lett.* 128:199–213

Jacob DE. 2004. Nature and origin of eclogite xenoliths from kimberlites. *Lithos* 77:295–316

Jacob DE, Bizimis M, Salters VJM. 2005. Lu–Hf and geochemical systematics of recycled ancient oceanic crust: evidence from Roberts Victor eclogites. *Contrib. Mineral. Petrol.* 148:707–20

Jacob DE, Piazolo S, Schreiber A, Trimby P. 2016. Redox-freezing and nucleation of diamond via magnetite formation in the Earth's mantle. *Nat. Commun.* 7:11891

Jagoutz O, Schmidt MW. 2013. The composition of the foundered complement to the continental crust and a re-evaluation of fluxes in arcs. *Earth Planet. Sci. Lett.* 371:177–90

Jenner FE, O'Neill HS. 2012. Analysis of 60 elements in 616 ocean floor basaltic glasses. *Geochem. Geophys. Geosyst.* 13:Q02005

Jerde EA, Taylor LA, Crozaz G, Sobolev NV, Sobolev VN. 1993. Diamondiferous eclogites from Yakutia, Siberia: evidence for a diversity of protoliths. *Contrib. Mineral. Petrol.* 114:189–202

John T, Scherer EE, Haase K, Schenk V. 2004. Trace element fractionation during fluid-induced eclogitization in a subducting slab: trace element and Lu–Hf–Sm–Nd isotope systematics. *Earth Planet. Sci. Lett.* 227:441–56

Jugo PJ, Luth RW, Richards JP. 2005. An experimental study of the sulfur content in basaltic melts saturated with immiscible sulfide or sulfate liquids at 1300°C and 1·0 GPa. *J. Petrol.* 46:783–98

Katayama I, Nakashima S, Yurimoto H. 2006. Water content in natural eclogite and implication for water transport into the deep upper mantle. *Lithos* 86:245–59

Kelemen PB, Manning CE. 2015. Reevaluating carbon fluxes in subduction zones, what goes down, mostly comes up. *PNAS* 112:E3997–4006

Kelley KA, Plank T, Grove TL, Stolper EM, Newman S, Hauri E. 2006. Mantle melting as a function of water content beneath back-arc basins. *J. Geophys. Res.* 111(B9):B09208

Koornneef JM, Bouman C, Schwieters JB, Davies GR. 2014. Measurement of small ion beams by thermal ionisation mass spectrometry using new 10(13) Ohm resistors. *Anal. Chim Acta* 819:49–55

Korolev N, Nikitina LP, Goncharov A, Dubinina EO, Melnik A, et al. 2021. Three types of mantle eclogite from two layers of oceanic crust: a key case of metasomatically-aided transformation of low-to-high-magnesian eclogite. *J. Petrol.* 62:egab070

Korolev NM, Kopylova M, Bussweiler Y, Pearson DG, Gurney J, Davidson J. 2018. The uniquely high-temperature character of Cullinan diamonds: a signature of the Bushveld mantle plume? *Lithos* 304:362–73

Kostrovitsky SI, Skuzovatov SY, Yakovlev DA, Sun J, Nasdala L, Wu F-Y. 2016. Age of the Siberian craton crust beneath the northern kimberlite fields: insights to the craton evolution. *Gondwana Res.* 39:365–85

Kylander-Clark ARC, Hacker BR, Mattinson CG. 2012. Size and exhumation rate of ultrahigh-pressure terranes linked to orogenic stage. *Earth Planet. Sci. Lett.* 321–322:115–20

Kyser TK. 2018. Stable isotope variations in the mantle. In *Stable Isotopes in High Temperature Geological Processes*, ed. JW Valley, HP Taylor, JR O'Neil, pp. 141–64. Berlin: De Gruyter

Lambart S, Baker MB, Stolper EM. 2016. The role of pyroxenite in basalt genesis: Melt-PX, a melting parameterization for mantle pyroxenites between 0.9 and 5 GPa. *J. Geophys. Res. Solid Earth* 121:5708–35

Lee CTA, Cheng X, Horodyskyj U. 2006. The development and refinement of continental arcs by primary basaltic magmatism, garnet pyroxenite accumulation, basaltic recharge and delamination: insights from the Sierra Nevada, California. *Contrib. Mineral. Petrol.* 151:222–42

Lehnert K, Su Y, Langmuir C, Sarbas B, Nohl U. 2000. A global geochemical database structure for rocks. *Geochem. Geophys. Geosyst.* 1:1012

Liu S-A, Qu Y-R, Wang Z-Z, Li M-L, Yang C, Li S-G. 2022. The fate of subducting carbon tracked by Mg and Zn isotopes: a review and new perspectives. *Earth-Sci. Rev.* 228:104010

Luo Y, Korenaga J. 2020. Efficiency of eclogite removal from continental lithosphere and its implications for cratonic diamonds. *Geology* 49:438–41

Luth RW, Stachel T. 2014. The buffering capacity of lithospheric mantle: implications for diamond formation. *Contrib. Mineral. Petrol.* 168:1083

Lyons TW, Reinhard CT, Planavsky NJ. 2014. The rise of oxygen in Earth's early ocean and atmosphere. *Nature* 506:307–15

Magni V, Bouilhol P, van Hunen J. 2014. Deep water recycling through time. *Geochem. Geophys. Geosyst.* 15:4203–16

Marschall HR, Wanless VD, Shimizu N, von Strandmann P, Elliott T, Monteleone BD. 2017. The boron and lithium isotopic composition of mid-ocean ridge basalts and the mantle. *Geochim. Cosmochim. Acta* 207:102–38

Mattey D, Lowry D, Macpherson C. 1994. Oxygen-isotope composition of mantle peridotite. *Earth Planet. Sci. Lett.* 128:231–41

Mazzone P, Haggerty SE. 1989. Peraluminous xenoliths in kimberlite: metamorphosed restites produced by partial melting of pelites. *Geochim. Cosmochim. Acta* 53:1551–61

McDonough WF. 1991. Chemical and isotopic systematics of continental lithospheric mantle. In *Kimberlites, Related Rocks and Mantle Xenoliths*, ed. HOA Meyer, OH Leonardos, pp. 478–85. Rio de Janeiro: Cia. Pesqui. Recur. Minerais

McDonough WF, Sun S-S. 1995. The composition of the Earth: chemical evolution of the mantle. *Chem. Geol.* 120:223–53

McGunnigle JP, Cano EJ, Sharp ZD, Muehlenbachs K, Cole D, et al. 2022. Triple oxygen isotope evidence for a hot Archean ocean. *Geology* 50(9):991–95

McIntyre T, Kublik K, Currie C, Pearson DG. 2021. Heat generation in cratonic mantle roots—new trace element constraints from mantle xenoliths and implications for cratonic geotherms. *Geochem. Geophys. Geosyst.* 22:e2021GC009691

Meyer HOA. 1987. Inclusions in diamond. In *Mantle Xenoliths*, ed. PH Nixon, pp. 501–22. Chichester, UK: Wiley & Sons

Mikhailenko D, Golovin A, Korsakov A, Aulbach S, Gerdes A, Ragozin A. 2020. Metasomatic evolution of coesite-bearing diamondiferous eclogite from the Udachnaya kimberlite. *Minerals* 10(4):383

Mikhailenko DS, Aulbach S, Korsakov AV, Golovin AV, Malygina EV, et al. 2021. Origin of graphite–diamond-bearing eclogites from Udachnaya kimberlite pipe. *J. Petrol.* 62:egab033

Mole DR, Fiorentini ML, Thebaud N, Cassidy KF, McCuaig TC, et al. 2014. Archean komatiite volcanism controlled by the evolution of early continents. *PNAS* 111:10083–88

Möller A, Appel P, Mezger K, Schenk V. 1995. Evidence for a 2 Ga subduction zone—eclogites in the Usagaran Belt of Tanzania. *Geology* 23:1067–70

Neal CR, Taylor LA, Davidson JP, Holden P, Halliday AN, et al. 1990. Eclogites with oceanic crustal and mantle signatures from the Bellsbank kimberlite, South Africa, part 2: Sr, Nd, and O isotope geochemistry. *Earth Planet. Sci. Lett.* 99:362–79

Nebel O, Sossi PA, Bénard A, Arculus RJ, Yaxley GM, et al. 2019. Reconciling petrological and isotopic mixing mechanisms in the Pitcairn mantle plume using stable Fe isotopes. *Earth Planet. Sci. Lett.* 521:60–67

Nicklas RW, Puchtel IS, Ash RD, Piccoli HM, Hanski E, et al. 2019. Secular mantle oxidation across the Archean-Proterozoic boundary: evidence from V partitioning in komatiites and picrites. *Geochim. Cosmochim. Acta* 250:49–75

Ning W, Kusky T, Wang L, Huang B. 2022. Archean eclogite-facies oceanic crust indicates modern-style plate tectonics. *PNAS* 119:e2117529119

Niu YL, O'Hara MJ. 2009. MORB mantle hosts the missing Eu (Sr, Nb, Ta and Ti) in the continental crust: new perspectives on crustal growth, crust–mantle differentiation and chemical structure of oceanic upper mantle. *Lithos* 112:1–17

O'Neill C, Aulbach S. 2022. Destabilization of deep oxidized mantle drove the Great Oxidation Event. *Sci. Adv.* 8:eabg1626

Palin RM, Dyck B. 2018. Metamorphic consequences of secular changes in oceanic crust composition and implications for uniformitarianism in the geological record. *Geosci. Front.* 9:1009–19

Pearson DG, Wittig N. 2014. The formation and evolution of cratonic mantle lithosphere—evidence from mantle xenoliths. See Holland et al. 2014, pp. 255–92

Pokhilenko L. 2021. Kelyphite rims on garnets of contrast parageneses in mantle xenoliths from the Udachnaya-East kimberlite pipe (Yakutia). *Minerals* 11:615

Rader E, Emry E, Schmerr N, Frost D, Cheng C, et al. 2015. Characterization and petrological constraints of the midlithospheric discontinuity. *Geochem. Geophys. Geosyst.* 16:3484–504

Radu IB, Moine BN, Bolfan-Casanova N, Ionov DA, Devidal JL, et al. 2022. Zoisite in cratonic eclogite xenoliths—implications for water in the upper mantle. *Lithos* 418–419:106681

Rapp RP, Watson EB. 1995. Dehydration melting of metabasalt at 8–32 kbar: implications for continental growth and crust-mantle recycling. *J. Petrol.* 36:891–931

Richardson SH, Gurney JJ, Erlank AJ, Harris JW. 1984. Origin of diamonds in old enriched mantle. *Nature* 310:198–202

Richardson SH, Shirey SB. 2008. Continental mantle signature of Bushveld magmas and coeval diamonds. *Nature* 453:910–13

Rogers JJW, Santosh M. 2003. Supercontinents in Earth history. *Gondwana Res.* 6:357–68

Rollinson H. 1997. Eclogite xenoliths in west African kimberlites as residues from Archaean granitoid crust formation. *Nature* 389:173–76

Rollinson H. 2016. Archaean crustal evolution in West Africa: a new synthesis of the Archaean geology in Sierra Leone, Liberia, Guinea and Ivory Coast. *Precambrian Res.* 281:1–12

Rudnick RL, Barth M, Horn I, McDonough WF. 2000. Rutile-bearing refractory eclogites: missing link between continents and depleted mantle. *Science* 287:278–81

Rudnick RL, Fountain DM. 1995. Nature and composition of the continental crust: a lower crustal perspective. *Rev. Geophys.* 33:267–309

Rudnick RL, Gao S. 2014. Composition of the continental crust. See Holland et al. 2014, pp. 1–51

Schmidberger SS, Simonetti A, Heaman LM, Creaser RA, Whiteford S. 2007. Lu-Hf, in-situ Sr and Pb isotope and trace element systematics for mantle eclogites from the Diavik diamond mine: evidence for Paleoproterozoic subduction beneath the Slave craton, Canada. *Earth Planet. Sci. Lett.* 254:55–68

Schmidt MW, Jagoutz O. 2017. The global systematics of primitive arcmelts. *Geochem. Geophys. Geosyst.* 18:2817–54

Schmidt MW, Poli S. 2014. Devolatilization during subduction. See Holland et al. 2014, pp. 669–701

Shchukina EV, Agashev AM, Zedgenizov DA. 2018. Origin of zircon-bearing mantle eclogites entrained in the V. Grib kimberlite (Arkhangelsk region, NW Russia): evidence from mineral geochemistry and the U-Pb and Lu-Hf isotope compositions of zircon. *Mineral. Petrol.* 112:85–100

Shirey SB, Richardson SH. 2011. Start of the Wilson cycle at 3 Ga shown by diamonds from subcontinental mantle. *Science* 333:434–36

Smart KA, Chacko T, Stachel T, Tappe S, Stern RA, et al. 2012. Eclogite formation beneath the northern Slave craton constrained by diamond inclusions: oceanic lithosphere origin without a crustal signature. *Earth Planet. Sci. Lett.* 319:165–77

Smart KA, Heaman LM, Chacko T, Simonetti A, Kopylova M, et al. 2009. The origin of high-MgO diamond eclogites from the Jericho kimberlite, Canada. *Earth Planet. Sci. Lett.* 284:527–37

Smart KA, Tappe S, Simonetti A, Simonetti SS, Woodland AB, Harris C. 2017. Tectonic significance and redox state of Paleoproterozoic eclogite and pyroxenite components in the Slave cratonic mantle lithosphere, Voyageur kimberlite, Arctic Canada. *Chem. Geol.* 455:98–119

Smart KA, Tappe S, Stern RA, Webb SJ, Ashwall LD. 2016. Early Archaean tectonics and mantle redox recorded in Witwatersrand diamonds. *Nat. Geosci.* 9:255–59

Smart KA, Tappe S, Woodland AB, Greyling DR, Harris C, Gussone N. 2021a. Constraints on Archean crust recycling and the origin of mantle redox variability from the $\delta^{44/40}Ca - \delta^{18}O - fO_2$ signatures of cratonic eclogites. *Earth Planet. Sci. Lett.* 556:116720

Smart KA, Tappe S, Woodland AB, Harris C, Corcoran L, Simonetti A. 2021b. Metasomatized eclogite xenoliths from the central Kaapvaal craton as probes of a seismic mid-lithospheric discontinuity. *Chem. Geol.* 578:120286

Smit KV, Stachel T, Luth RW, Stern RA. 2019. Evaluating mechanisms for eclogitic diamond growth: an example from Zimmi Neoproterozoic diamonds (West African craton). *Chem. Geol.* 520:21–32

Soderman CR, Shorttle O, Matthews S, Williams HM. 2022. Global trends in novel stable isotopes in basalts: theory and observations. *Geochim. Cosmochim. Acta* 318:388–414

Sommer H, Jacob DE, Stern RA, Petts D, Mattey DP, Pearson DG. 2017. Fluid-induced transition from banded kyanite- to bimineralic eclogite and implications for the evolution of cratons. *Geochim. Cosmochim. Acta* 207:19–42

Spetsius ZV, Taylor LA. 2002. Partial melting in mantle eclogite xenoliths: connections with diamond paragenesis. *Int. Geol. Rev.* 44:973–87

Stachel T, Aulbach S, Harris JW. 2022. Mineral inclusions in lithospheric diamonds. *Rev. Mineral. Geochem.* 88:307–91

Stachel T, Harris JW. 2008. The origin of cratonic diamonds—constraints from mineral inclusions. *Ore Geol. Rev.* 34:5–32

Stagno V, Frost DJ, McCammon CA, Mohseni H, Fei Y. 2015. The oxygen fugacity at which graphite or diamond forms from carbonate-bearing melts in eclogitic rocks. *Contrib. Mineral. Petrol.* 169:16

Stagno V, Ojwang DO, McCammon CA, Frost DJ. 2013. The oxidation state of the mantle and the extraction of carbon from Earth's interior. *Nature* 493:84–88

Stolper DA, Keller CB. 2018. A record of deep-ocean dissolved O_2 from the oxidation state of iron in submarine basalts. *Nature* 553:323–27

Stracke A. 2012. Earth's heterogeneous mantle: a product of convection-driven interaction between crust and mantle. *Chem. Geol.* 330:274–99

Stracke A. 2021. A process-oriented approach to mantle geochemistry. *Chem. Geol.* 579:120350
Stracke A, Tipper ET, Klemme S, Bizimis M. 2018. Mg isotope systematics during magmatic processes: intermineral fractionation in mafic to ultramafic Hawaiian xenoliths. *Geochim. Cosmochim. Acta* 226:192–205
Sun S-s, McDonough WF. 1989. Chemical and isotopic systematics of oceanic basalts: implications for mantle composition and processes. In *Magmatism in the Ocean Basins*, ed. AD Saunders, MJ Norry, pp. 313–45. London: Geol. Soc.
Tamblyn R, Brown D, Hand M, Morrissey L, Clark C, Anczkiewicz R. 2021. The 2 Ga eclogites of Central Tanzania: directly linking age and metamorphism. *Lithos* 380–381:105890
Tao R, Zhang L, Zhang L. 2020. Redox evolution of western Tianshan subduction zone and its effect on deep carbon cycle. *Geosci. Front.* 11:915–24
Tappe S, Smart K, Torsvik T, Massuyeau M, de Wit M. 2018. Geodynamics of kimberlites on a cooling Earth: clues to plate tectonic evolution and deep volatile cycles. *Earth Planet. Sci. Lett.* 484:1–14
Tappe S, Smart KA, Pearson DG, Steenfelt A, Simonetti A. 2011. Craton formation in Late Archean subduction zones revealed by first Greenland eclogites. *Geology* 39:1103–6
Tatsumi Y, Hamilton DL, Nesbitt RW. 1986. Chemical characteristics of fluid phase released from a subducted lithosphere and origin of arc magmas: evidence from high-pressure experiments and natural rocks. *J. Volcanol. Geotherm. Res.* 29:293–309
Thomson AR, Kohn SC, Prabhu A, Walter MJ. 2021. Evaluating the formation pressure of diamond-hosted majoritic garnets: a machine learning majorite barometer. *J. Geophys. Res. Solid Earth* 126:e2020JB020604
Tsujimori T, Mattinson C. 2021. Eclogites in different tectonic settings. In *Encyclopedia of Geology*, ed. D Alderton, SA Elias, pp. 561–68. Oxford, UK: Academic, 2nd ed.
Viljoen KS. 1995. Graphite-bearing and diamond-bearing eclogite xenoliths from the Bellsbank kimberlites, Northern Cape, South Africa. *Contrib. Mineral. Petrol.* 121:414–23
Viljoen KS, Smith CB, Sharp ZD. 1996. Stable and radiogenic isotope study of eclogite xenoliths from the Orapa kimberlite, Botswana. *Chem. Geol.* 131:235–55
Wang SJ, Teng FZ, Rudnick RL, Li SG. 2015. Magnesium isotope evidence for a recycled origin of cratonic eclogites. *Geology* 43:1071–74
Wang Z, Kusky TM, Wang L. 2022. Long-lasting viscous drainage of eclogites from the cratonic lithospheric mantle after Archean subduction stacking. *Geology* 50:583–87
Wang Z-Z, Liu S-A, Rudnick RL, Teng F-Z, Wang S-J, Haggerty SE. 2022. Zinc isotope evidence for carbonate alteration of oceanic crustal protoliths of cratonic eclogites. *Earth Planet. Sci. Lett.* 580:117394
Waterton P, Guotana JM, Nishio I, Morishita T, Tani K, et al. 2022. No mantle residues in the Isua Supracrustal Belt. *Earth Planet. Sci. Lett.* 579:117348
Weiss Y, Czas J, Navon O. 2022. Fluid inclusions in fibrous diamonds. *Rev. Mineral. Geochem.* 88:475–532
White WM, Klein EM. 2014. Composition of the oceanic crust. See Holland et al. 2014, pp. 457–96
Wilson AH, Zeh A, Gerdes A. 2017. *In situ* Sr isotopes in plagioclase and trace element systematics in the lowest part of the eastern Bushveld Complex: dynamic processes in an evolving magma chamber. *J. Petrol.* 58:327–60
Zeh A, Gerdes A, Barton JM. 2009. Archean accretion and crustal evolution of the Kalahari Craton—the zircon age and Hf isotope record of granitic rocks from Barberton/Swaziland to the Francistown Arc. *J. Petrol.* 50:933–66

Annual Review
of Earth and
Planetary Sciences
Volume 51, 2023

Contents

Errata

An online log of corrections to *Annual Review of Earth and Planetary Sciences* articles may be found at http://www.annualreviews.org/errata/earth

Related Articles

From the ***Annual Review of Astronomy and Astrophysics***, Volume 60 (2022)

Atmospheres of Rocky Exoplanets
Robin Wordsworth and Laura Kreidberg

From the ***Annual Review of Chemical and Biomolecular Engineering***, Volume 13 (2022)

Direct Air Capture of CO_2 Using Solvents
Radu Custelcean

Technological Options for Direct Air Capture: A Comparative Process Engineering Review
Xiaowei Wu, Ramanan Krishnamoorti, and Praveen Bollini

From the ***Annual Review of Ecology, Evolution, and Systematics***, Volume 53 (2022)

Evolutionary Ecology of Fire
Jon E. Keeley and Juli G. Pausas

Integrating Fossil Observations Into Phylogenetics Using the Fossilized Birth–Death Model
April M. Wright, David W. Bapst, Joëlle Barido-Sottani, and Rachel C.M. Warnock

The Macroevolutionary History of Bony Fishes: A Paleontological View
Matt Friedman

From the ***Annual Review of Environment and Resources***, Volume 47 (2022)

The Ocean Carbon Cycle
Tim DeVries

Permafrost and Climate Change: Carbon Cycle Feedbacks From the Warming Arctic
Edward A.G. Schuur, Benjamin W. Abbott, Roisin Commane, Jessica Ernakovich, Eugenie Euskirchen, Gustaf Hugelius, Guido Grosse, Miriam Jones, Charlie Koven, Victor Leshyk, David Lawrence, Michael M. Loranty, Marguerite Mauritz, David Olefeldt, Susan Natali, Heidi Rodenhizer, Verity Salmon, Christina Schädel, Jens Strauss, Claire Treat, and Merritt Turetsky

Remote Sensing the Ocean Biosphere
Sam Purkis and Ved Chirayath

From the ***Annual Review of Fluid Mechanics***, Volume 55 (2023)

Submesoscale Dynamics in the Upper Ocean
John R. Taylor and Andrew F. Thompson

Fluid Dynamics of Polar Vortices on Earth, Mars, and Titan
Darryn W. Waugh

Icebergs Melting
Claudia Cenedese and Fiamma Straneo

The Fluid Mechanics of Deep-Sea Mining
Thomas Peacock and Raphael Ouillon

Turbulent Rotating Rayleigh–Bénard Convection
Robert E. Ecke and Olga Shishkina

From the ***Annual Review of Marine Science***, Volume 15 (2023)

From Stamps to Parabolas
S. George Philander

Sociotechnical Considerations About Ocean Carbon Dioxide Removal
Sarah R. Cooley, Sonja Klinsky, David R. Morrow, and Terre Satterfield

Nuclear Reprocessing Tracers Illuminate Flow Features and Connectivity Between the Arctic and Subpolar North Atlantic Oceans
Núria Casacuberta and John N. Smith

The Arctic Ocean's Beaufort Gyre
Mary-Louise Timmermans and John M. Toole

Global Quaternary Carbonate Burial: Proxy- and Model-Based Reconstructions and Persisting Uncertainties
Madison Wood, Christopher T. Hayes, and Adina Paytan

Quantifying the Ocean's Biological Pump and Its Carbon Cycle Impacts on Global Scales
David A. Siegel, Timothy DeVries, Ivona Cetinić, and Kelsey M. Bisson

Novel Insights into Marine Iron Biogeochemistry from Iron Isotopes
Jessica N. Fitzsimmons and Tim M. Conway

Insights from Fossil-Bound Nitrogen Isotopes in Diatoms, Foraminifera, and Corals
Rebecca S. Robinson, Sandi M. Smart, Jonathan D. Cybulski, Kelton W. McMahon, Basia Marcks, and Catherine Nowakowski

Prokaryotic Life in the Deep Ocean's Water Column
Gerhard J. Herndl, Barbara Bayer, Federico Baltar, and Thomas Reinthaler

Lipid Biogeochemistry and Modern Lipidomic Techniques
Bethanie R. Edwards

From the ***Annual Review of Materials Research***, Volume 52 (2022)

Biomineralized Materials for Sustainable and Durable Construction
Danielle N. Beatty, Sarah L. Williams, and Wil V. Srubar III

Brittle Solids: From Physics and Chemistry to Materials Applications
Brian R. Lawn and David B. Marshall

Material Flows and Efficiency
Jonathan M. Cullen and Daniel R. Cooper

Architectural Glass
Sheldon M. Wiederhorn and David R. Clarke